NACA RM L9D08

NACA

RESEARCH MEMORANDUM

ESTIMATED TRANSONIC FLYING QUALITIES OF A TAILLESS AIRPLANE BASED ON A MODEL INVESTIGATION

By

Charles J. Donlan and Richard E. Kuhn

Langley Aeronautical Laboratory
Langley Air Force Base, Va.

NATIONAL ADVISORY COMMITTEE
FOR AERONAUTICS

WASHINGTON

June 8, 1949
Declassified November 8, 1957

NATIONAL ADVISORY COMMITTEE FOR AERONAUTICS

RESEARCH MEMORANDUM

ESTIMATED TRANSONIC FLYING QUALITIES OF A TAILLESS AIRPLANE BASED ON A MODEL INVESTIGATION

By Charles J. Donlan and Richard E. Kuhn

SUMMARY

An analysis of the estimated flying qualities of a tailless airplane with the wing quarter-chord line swept back 35° in the Mach number range from 0.40 to 0.91 has been made, based on tests of a model of this airplane in the Langley high-speed 7- by 10-foot tunnel.

The analysis indicates longitudinal-control position instability at transonic speeds but the accompanying trim changes are not large. Control-position maneuvering stability, however, is present for all speeds. Longitudinal and lateral control appear adequate, but the damping of the short-period longitudinal and lateral oscillations at high altitudes is poor and would probably require artificial damping.

INTRODUCTION

Stability and control tests of a tailless-type swept-wing airplane model have been conducted in the Langley high-speed 7- by 10-foot tunnel through the Mach number range from 0.40 to 0.91. The flying qualities that might be expected from such an airplane have been estimated from these data for assumed wing loadings of 24 and 34 pounds per square foot at sea level and at an altitude of 40,000 feet. All computations are based on a center-of-gravity position of 17 percent of the mean aerodynamic chord.

The estimated flying qualities of the airplane are presented in the body of the paper and in figures 1 to 23. A discussion of the wind-tunnel tests is presented in the Appendix and the data are presented in figures 24 to 41.

COEFFICIENTS AND SYMBOLS

The system of axes employed, together with an indication of the positive forces, moments, and angles, is presented in figure 1. Pertinent symbols used in this paper are defined as follows:

C_L	lift coefficient (Lift/qS)
C_D	drag coefficient (Drag/qS)
C_m	pitching-moment coefficient (Pitching moment/$qS\bar{c}$)
C_l	rolling-moment coefficient (Rolling moment/qSb)
C_Y	side-force coefficient (Side force/qS)
C_n	yawing-moment coefficient (Yawing moment/qSb)
q	free-stream dynamic pressure, pounds per square foot $\left(\frac{\rho V^2}{2}\right)$
S	wing area
$\bar{c}$	wing mean aerodynamic chord (M.A.C.) $\left(\bar{c} = \frac{2}{S}\int_0^{b/2} c^2 db\right)$
c	chord, parallel to plane of symmetry
b	wing span
V	air velocity, feet per second
p	rolling velocity, degrees or radians per second
r	yawing velocity, radians per second
q	pitching velocity, radians per second
a	speed of sound, feet per second
M	Mach number (V/a)
R	Reynolds number $\left(\frac{\rho V \bar{c}}{\mu}\right)$
μ	absolute viscosity, pounds-seconds per square foot
ρ	mass density of air, slugs per cubic foot
α	angle of attack, measured from X-axis to fuselage center line, degrees
α_{static}	angle of attack of model under no-load conditions
δ	control deflection, measured on chord line parallel to the plane of symmetry, degrees
ψ	angle of yaw, degrees

β angle of sideslip, radians

η angle of attack of principal longitudinal axis of airplane, positive when principal axis is above flight path at the nose, degrees

ϵ angle between fueselage center line and principal axis of inertia, positive when fuselage center line is above principal axis, degrees

γ angle of flight path to horizontal axis, positive in climb, degrees

L/D lift-drag ratio $\left(C_L/C_D\right)$

W/S wing loading (Weight/S)

$$C_{m_\delta} = \frac{\partial C_m}{\partial \delta}$$

$$C_{l_\psi} = \frac{\partial C_l}{\partial \psi}$$

$$C_{n_\psi} = \frac{\partial C_n}{\partial \psi}$$

$$C_{Y_\psi} = \frac{\partial C_Y}{\partial \psi}$$

$$C_{l_p} = \frac{\partial C_l}{\partial\left(\frac{pb}{2V}\right)}$$

$$C_{n_p} = \frac{\partial C_n}{\partial\left(\frac{pb}{2V}\right)}$$

$$C_{Y_p} = \frac{\partial C_Y}{\partial\left(\frac{pb}{2V}\right)}$$

$$C_{l_r} = \frac{\partial C_l}{\partial\left(\frac{rb}{2V}\right)}$$

$$C_{n_r} = \frac{\partial C_n}{\partial\left(\frac{rb}{2V}\right)}$$

$$C_{Y_r} = \frac{\partial C_Y}{\partial\left(\frac{rb}{2V}\right)}$$

$$C_{L_\alpha} = \frac{\partial C_L}{\partial \alpha}$$

$$C_{m_q} = \frac{\partial C_m}{\partial\left(\frac{q\bar{c}}{2V}\right)}$$

k_{X_o} radius of gyration in roll about body axes, feet

k_{Y_o} radius of gyration in pitch about body axes, feet

k_{Z_o} radius of gyration in yaw about body axes, feet

Subscripts:

a aileron

l left

r right

MODEL AND AIRPLANE

The test model represented a tailless, swept-wing, jet-propelled, fighter-type airplane. The physical characteristics of the solid-steel model are presented in figure 2, and pictures of the model mounted on the sting-support systems used for this investigation are presented in figure 3. For the portions of analysis for which full-scale airplane dimensions were required, a model scale of 0.08 was assumed. The control surfaces, which are plain flaps with sealed gaps, are intended to be used for both longitudinal and lateral control. Rudders were not simulated on the model. Air flow through the jet-intake ducts was permitted for all tests, and one of the exhaust ports, together with its mirror image, can be seen in figure 3(a).

BASIS OF ANALYSIS

The most recent specification for satisfactory flying qualities (reference 1) has been used as a guide in the present analysis. However, inasmuch as the analysis is restricted to the high-speed configuration without regard to control forces (no model hinge-moment data were obtained) and because much of the interest centers about the behavior of the airplane at speeds above those at which adverse compressibility effects are encountered, no detailed step-by-step comparison with the specifications has been attempted.

The estimated characteristics of the aircraft at each Mach number are based upon the results of tunnel tests at the same Mach number but at the test Reynolds number indicated in figure 4. The full-scale Reynolds numbers corresponding to flight at sea level and at an altitude of 40,000 feet are also shown in figure 4. No attempt was made to account for Reynolds number effects in interpreting the results. It is of interest to note, however, that a few unpublished tests made with transition fixed at the leading edge in order to simulate flow conditions at high Reynolds numbers were in good agreement with the basic free-transition tests. This indicates that, although the bulk of the data was obtained with free transition, the model data were not obtained in a critical range of Reynolds number.

RESULTS AND DISCUSSION

Performance

Flight conditions.- The variations with Mach number of the lift coefficient required for level flight for the various wing loadings and altitudes considered in the analysis are given in figure 5 and the corresponding angle-of-attack variation is given in figure 6. Figure 6 is useful for estimating the inclination of the principal axes of inertia for the different flight conditions. It will be observed that the angle of attack for level flight at sea level for the lighter wing loading becomes slightly negative at the highest Mach numbers. This condition, of course, is a result of the shift in angle of zero lift effected by the deflected elevator required for balance.

Lift-drag ratios.- The variation of the untrimmed lift-drag ratios at the various Mach numbers as a function of the lift coefficient is presented in figure 7. It will be observed that the lift coefficient for maximum L/D is essentially independent of Mach number, although the magnitude of the available L/D maximum drops rather rapidly above a Mach number of 0.80. The level-flight L/D values associated with the trimmed-flight conditions defined in figure 5 are presented in figure 8. The advantages to be gained by flying at high altitude are forcefully illustrated by this figure.

Longitudinal Stability and Control

Strictly speaking the elevator deflections for the various configurations discussed in the following paragraphs are slightly in error (about 1/3 of a deg too much down elevator) because the data used in the analysis were not corrected for the additional pitching-moment correction discussed in the appendix.

Static longitudinal stability.- The static longitudinal stability of the airplane is presented in figure 9 in the form of the variation of the elevator position required for trim with Mach number. Control-position instability is first manifested at a Mach number of 0.90 at sea level and at a Mach number of 0.85 at an altitude of 40,000 feet. The causes of the control-position instability exhibited above these Mach numbers are traceable to the rapid changes occurring in the basic untrimmed pitching-moment coefficient (fig. 10(a)) and to the changes in control effectiveness (fig. 10(b)). The resultant changes in trim, however, appear to be relatively gradual and of moderate magnitude, at least to a Mach number of 0.91, and may not be objectionable.

A rigorous evaluation of the neutral-point location (center-of-gravity position for which $\frac{d\delta}{dM} = 0$) at these Mach numbers would indeed indicate that the control-fixed neutral point moves well ahead of the center-of-gravity position. However, the utility of the neutral-point concept largely vanishes when irregular and rapid changes in trim occur. The desired information on static longitudinal stability appears to be most directly conveyed through charts like figure 9.

Maneuvering stability.- For tailless aircraft which possess very little damping in pitch, the factor $\left(\frac{\partial C_m}{\partial C_L}\right)_M$ very nearly defines the stick-fixed "maneuver margin" - the distance, expressed as a fraction of the chord, that the center of gravity is ahead of the "maneuver point." (The maneuver point is the center-of-gravity position for which the rate of change of control deflection with normal acceleration vanishes.)

The variation of the maneuver-point location with Mach number is presented for several lift coefficients in figure 11. It is evident that the maneuver point moves rearward, in general, at the higher Mach numbers. However, because of the nonlinearities involved in the evaluation of the maneuver point, its influence can be studied more conveniently in conjunction with the evaluation of the effectiveness of the longitudinal control.

Longitudinal-control effectiveness.- The amount of elevator control required for various accelerated-flight conditions is presented in figure 12. For flight at sea level (figs. 12(c) and 12(d)), only

about 1° of elevator is required to produce a 6g acceleration at a Mach number of 0.85. The elevator must always be moved in the desired direction, however, as would be expected from the maneuver-point movement previously discussed (fig. 11). The minimum degree of stick-position maneuvering stability that can be tolerated will depend on the associated stick-force gradient. A small stick-position gradient, however, may make it difficult to design the control system to supply an adequate force gradient and still keep the maximum control force for other conditions within the capabilities of the pilot. At altitude of 40,000 feet (figs. 12(a) and 12(b)), much larger control deflections are required for the accelerated-flight conditions which makes the design of the control system even more critical.

Dynamic stability.- The characteristics of the stick-fixed short-period longitudinal oscillation are presented in figures 13 to 16. The computations are based on the formulas of reference 2 and the appropriate parameters in table I. While it is desirable that the short-period oscillation be damped to one-tenth amplitude in one cycle, it is obvious from figure 16 that this tailless design would not meet such a requirement at altitude. For the altitude case, it is seen that an oscillation of about 40 percent of the original amplitude still persists after one complete oscillation. At sea level, on the other hand, the damping of the oscillation appears to be adequate.

The damping characteristics have been evaluated for the control-fixed condition although the specifications are based upon free controls. However, if an irreversible control system were used on this airplane, the fixed-control characteristics would dictate the behavior of the aircraft.

Lateral Stability and Control

Lateral stability parameters.- Because of the absence of any rudder data from which trimmed yawed conditions could be evaluated, the directional and lateral stability will be adjudged from the stability parameters presented in figure 17. In general, the data indicate adequate static lateral stability. It will be noted, however, that the speed brakes decrease the directional stability and produce a slight negative dihedral effect $\left(\text{negative } C_{l_\psi}\right)$ at the highest Mach numbers.

Lateral control.- The lateral-control characteristics of the airplane are presented in figure 18 in the form of the variation with Mach number of the wing-tip helix angle $\frac{pb}{2V}$ obtained with various total aileron deflections. The helix angle was computed from the simple relation $\frac{pb}{2V} = -\frac{C_l}{C_{l_p}}$ using the aileron rolling-moment data presented in

figure 34 and the damping characteristics given in figure 18. The damping coefficients were estimated by the method of reference 3. Some unpublished experimental C_{l_p} data indicate that for this wing plan form the theoretical values are in good agreement with experiment.

The rate of roll expressed in degrees per second is presented in figure 19. Aeroelastic distortion effects would undoubtedly decrease the rates of roll from those indicated in figure 19, but in any event the rates of roll should be extremely high. It will be noted that, as in the case of longitudinal control, lateral-control effectiveness begins to decrease rapidly at the highest Mach numbers.

It is evident from the extremely rapid rates of roll possible on this airplane that the limiting rate of roll will probably be conditioned by the pilot's ability to withstand the angular accelerations imposed.

Dynamic stability.- Using the parameters presented in table I, the characteristics of the control-fixed lateral oscillations have been evaluated by the method of reference 4 and are presented in figures 20 to 23. The values of C_{l_p} presented in this table are slightly different from those given in figure 18, but the effect of this difference on the dynamic stability characteristics was found to be negligible.

It will be noted from figure 23 that the damping of the oscillation is marginal for the sea-level conditions and is definitely unsatisfactory for the altitude conditions according to the desired damping criterion set forth in reference 1. If flight tests on airplanes of this type subsequently demonstrate the real need for additional damping, the simplest way to provide for it would be to introduce artificial damping into the system in the form of rudder control coupled to a gyroscope sensitive to yawing velocity as discussed, for example, in reference 5.

A check on spiral stability was also made for the conditions stated in figure 20. It was found that spiral instability was present at a Mach number above 0.9, but the degree of spiral instability was so slight that the time required for the angle of bank to increase 10 percent was of the order of 1 minute at an altitude of 40,000 feet and 4 minutes at sea level.

CONCLUSIONS

An analysis of the transonic flying qualities to be expected from a tailless airplane in the Mach number range from 0.40 to 0.91 based on a model investigation indicates the following conclusions:

1. The airplane would exhibit longitudinal control-position instability at transonic speeds but the accompanying trim changes at these speeds should not be large.

2. Control-position maneuvering stability would be present at all speeds investigated although the control-position gradient may be as high as 6g's per degree of elevator deflection at low altitudes.

3. The damping of the short-period longitudinal oscillation at high altitudes would be less than desired.

4. The damping of the lateral oscillation at high altitude would be very poor and would probably require artificial damping.

5. Longitudinal and lateral control appear to be adequate at all speeds investigated.

Langley Aeronautical Laboratory
National Advisory Committee for Aeronautics
Langley Air Force Base, Va.

APPENDIX

WIND-TUNNEL INVESTIGATION

Tests

Scope.- The tests covered a Mach number range of 0.40 to 0.91 and an angle-of-attack range of 0° to 10°. Yaw tests were conducted through $\pm 4^\circ$ at 0° and 6° angle of attack. Longitudinal-control tests were conducted for -4.4° to 9.5° elevator deflection through the angle-of-attack and Mach number range, and aileron-control tests covered -1.8° to 18.9° deflection of the left aileron through the angle-of-attack and Mach number range. The effect of the fins, canopy, and speed brakes on the longitudinal and lateral stability and control was also investigated.

The variation of test Reynolds number with Mach number for average test conditions is presented in figure 4. The size of the model used in the present investigation resulted in a corrected tunnel choking Mach number of about 0.94. Experience has indicated that, with this value of choking Mach number, the data should be reliable up to a corrected Mach number of about 0.91.

Support system.- The model was supported by a sting extending from the rear of the fuselage to a vertical strut located behind the model. A photograph of the model supported on this system is shown in figure 3(a). The tare forces and moments produced by the center sting were determined by mounting the model on two wing supports which were also attached to the vertical strut and testing the model with and without the center sting (fig. 3(b)). For wing-alone tests the method that was employed to obtain pitching-moment tares was found to give unreliable results. Consequently, no pitching-moment data for the wing alone are presented in this report. Angles of attack and yaw were changed by the use of interchangeable couplings in the stings behind the model. Deflections of the support system under load were determined from static-loading tests.

Corrections.- The test results have been corrected for tare forces and moments produced by the support system. However, there are small additional corrections to the pitching-moment and rolling-moment coefficients which have not been incorporated in the data. These corrections, which are inherent in the balance system, were determined subsequent to the completion of the present investigation, but the data of this paper can be corrected as follows:

$$(C_m)_{\text{corrected}} = (C_m)_{\text{presented}} - 0.003$$

$$(C_l)_{\text{corrected}} = (C_l)_{\text{presented}} - 0.0008$$

The jet-boundary corrections to the lift and drag were computed by the method of reference 6. The jet-boundary corrections to other components were considered negligible.

The drag has been corrected for the buoyancy produced by the small longitudinal static-pressure gradient in the tunnel. All coefficients and Mach numbers were corrected for blocking by the model and its wake by the method of reference 7.

RESULTS AND DISCUSSION

The results of the wind-tunnel tests are presented in the following figures. The pitching-moment coefficients are presented about a center of gravity located at 17 percent of the mean aerodynamic chord.

Basic Force Data:	Figure
Longitudinal -	
Pitch tests, effect of control deflection, speed brakes, fins, canopy, and wing-alone data	24, 25, 26
Lift-curve slope	27
Curves of $\left(\frac{\partial C_m}{\partial C_L}\right)_M$	28
Control effectiveness parameter	29
Lateral -	
Yaw tests, effect of speed brakes, fins, canopy, and wing-alone data	30, 31
Lift coefficient of yaw tests	32
Lateral-stability derivatives	33
Lateral-control tests	34
Effect of aileron deflection on drag	35
Effect of fins on aileron effectiveness	36
Miscellaneous Data:	
Tuft studies of flow over wing	37
Speed-brake configurations -	
Drawing of fuselage brakes	38
Tuft studies	39
Effect on lift, drag, and pitching moment	40
Drag increments	41

Longitudinal stability and control.- The aerodynamic characteristics in pitch of the model and various components are presented in figures 24, 25, and 26. For these tests a cluster of static and total head tubes was installed in the right duct to measure the flow during tests. The inlet-velocity ratios measured were small compared to those which might be expected in flight; however, calculations have indicated that only a small pitching moment results from turning the inlet air through the angle of attack at the duct inlet.

Visual observation of tufts indicated no external flow separation from the duct inlets at any Mach number at low angles of attack. At the highest angle of attack, however, a local separation from the upper surface of the duct lip was observed at Mach numbers as low as 0.45 (fig. 37).

The elevator effectiveness parameter C_{m_δ} (fig. 10(b)) was determined from cross plots of the data from figure 24 and is defined as the slope of the pitching-moment coefficient plotted against elevator-deflection curve at zero elevator deflection. The pitching-moment coefficient was found to vary linearly with deflection through the deflection range at the lower Mach numbers. At large deflections the effectiveness was somewhat reduced at the higher Mach numbers.

The effectiveness parameter $\left(\frac{\Delta C_m}{\Delta \delta}\right)_{0^\circ \text{ to } 4.4^\circ}$ (fig. 29) is based on data obtained from elevator deflections 0° and -4.4° only.

Lateral stability.- The variation of lateral-stability characteristics with Mach number ($\alpha_{static} = 0^\circ$ and 6°) for several configurations of the model are presented in figures 30 and 31. During the test runs in which these data were obtained, the lift coefficient varied as indicated by the curves in figure 32. The angle-of-attack change from the wind-off static values ($\alpha_{static} = 0^\circ$ and 6°) was caused by the deflection of the support system under aerodynamic load and is indicated by the values of the actual angle of attack shown in figure 32.

Lateral control.- Most of the test results presented are for the complete model configuration consisting of the wing, fuselage, canopy, and vertical tails (figs. 34 and 35). Several tests, however, were made with the vertical tails removed (fig. 36) and these data are uncorrected for the small changes in angle of attack of the model caused by deflection of the sting-support system. The data, however, can be compared with those of figure 34 inasmuch as the lateral characteristics are not particularly sensitive to angle of attack in this range.

It is of interest to note that at low angles of attack there is an appreciable favorable yawing moment accompanying the large negative aileron deflections at all Mach numbers and that this yawing moment decreases with increase of angle of attack. A study of the data indicates that this favorable yawing moment is attributable to the side force on the vertical fins induced by the deflected aileron. The decrease in yawing moment with increase in angle of attack is probably caused by the variation with angle of attack of the incremental-drag coefficient produced by the aileron. (See fig. 35.)

Speed-brake modifications.- Tuft studies of the flow over the model with the original speed brakes (fig. 39(a)) indicated bad separation of the flow over the vertical fins, particularly the inboard surface, over

most of the Mach number range. In an effort to improve this condition, other speed-brake configurations (fig. 38) were tested. On the basis of these tuft observations (figs. 39(b), 39(c), and 39(d)), it appeared that all the modifications tested eliminated the poor flow conditions evident at the vertical fin with the original configuration.

The effect of these speed-brake configurations on the aerodynamic characteristics in pitch is presented in figure 40 for a static angle of attack of 1.8°. The variation of the drag increments (ΔC_D), produced by the various speed brakes, with Mach number is presented in figure 41. It is evident from these data that the modified wing brakes produced considerably larger drag increments than the fuselage brakes.

REFERENCES

1. Anon.: Specification for Flying Qualities of Piloted Airplanes. NAVAER SR-119B, Bur. Aero., June 1, 1948.

2. Greenberg, Harry, and Sternfield, Leonard: A Theoretical Investigation of Longitudinal Stability of Airplanes with Free Controls Including Effect of Friction in Control System. NACA Rep. No. 791, 1944.

3. Swanson, Robert S., and Priddy, E. LaVerne: Lifting-Surface-Theory Values of the Damping in Roll and of the Parameter Used in Estimating Aileron Stick Forces. NACA ARR No. L5F23, 1945.

4. Sternfield, Leonard: Some Considerations of the Lateral Stability of High-Speed Aircraft. NACA TN No. 1282, 1947.

5. Sternfield, Leonard: Effect of Automatic Stabilization on the Lateral Oscillatory Stability of a Hypothetical Airplane at Supersonic Speeds. NACA TN No. 1818, 1949.

6. Gillis, Clarence L., Polhamus, Edward C., and Gray, Joseph L., Jr.: Charts for Determining Jet-Boundary Corrections for Complete Models in 7- by 10-Foot Closed Rectangular Wind Tunnels. NACA ARR No. L5G31, 1945.

7. Herriot, John G.: Blockage Corrections for Three-Dimensional-Flow Closed-Throat Wind Tunnels, with Consideration of the Effect of Compressibility. NACA RM No. A7B28, 1947.

TABLE I

PARAMETERS USED IN DYNAMIC STABILITY COMPUTATIONS

$\left[\epsilon = 0;\ \gamma = 0;\ C_{Y_p} = 0;\ C_{Y_r} = 0\right]$

W/S	Altitude	M	η	C_L	Longitudinal			Lateral								
					C_{m_q}	C_{m_α}	$\frac{kY_o}{\bar{c}}$	$\frac{kX_o}{b}$	$\frac{kZ_o}{b}$	C_{l_p}	C_{l_r}	C_{n_p}	C_{n_r}	C_{l_β}	C_{n_β}	C_{Y_β}
24	Sea level	0.4	1.75	0.1	-0.724	-0.312	0.575	0.145	0.243	-0.240	0.0228	-0.0055	-0.0604	-0.0344	0.0573	-0.372
24	Sea level	.5	.85	.067	-.756	-.313	.575	.145	.243	-.245	.0152	-.0037	-.0653	-.0172	.0516	-.401
24	Sea level	.6	.4	.046	-.787	-.314	.575	.145	.243	-.251	.0104	-.0026	-.0704	-.0086	.0487	-.430
24	Sea level	.7	.25	.038	-.835	-.322	.575	.145	.243	-.256	.0085	-.0024	-.0757	-.0057	.0458	-.458
24	Sea level	.8	.1	.025	-.918	-.341	.575	.145	.243	-.265	.0055	-.0018	-.0810	-.0040	.0573	-.487
24	Sea level	.85	0	.021	-.972	-.3791	.575	.145	.243	-.269	.0046	-.0018	-.0836	-.0023	.0630	-.516
24	Sea level	.875	-.05	.020	-1.005	-.447	.575	.145	.243	-.271	.0044	-.0018	-.0848	-.0011	.0688	-.516
24	Sea level	.9	-.1	.019	-1.036	-.565	.575	.145	.243	-.275	.0041	-.0020	-.0866	0	.0716	-.487
24	Sea level	.91	0	.019	-1.049	-.654	.575	.145	.243	-.278	.0041	-.0021	-.0881	0	.0745	-.487
24	40,000 feet	.6	4.23	.243	-.787	-.314	.575	.145	.243	-.251	.0547	-.0139	-.0730	-.0688	.0620	-.430
24	40,000 feet	.7	2.90	.181	-.835	-.322	.575	.145	.243	-.256	.0404	-.0113	-.0769	-.0487	.0573	-.458
24	40,000 feet	.8	1.95	.138	-.918	-.341	.575	.145	.243	-.265	.0305	-.0101	-.0818	-.0372	.0573	-.487
24	40,000 feet	.85	1.60	.122	-.972	-.379	.575	.145	.243	-.269	.0268	-.0102	-.0841	-.0258	.0630	-.516
24	40,000 feet	.875	1.45	.115	-1.005	-.447	.575	.145	.243	-.271	.0251	-.0104	-.0858	-.0201	.0688	-.516
24	40,000 feet	.9	1.35	.110	-1.036	-.565	.575	.145	.243	-.275	.0239	-.0113	-.0879	-.0143	.0716	-.487
24	40,000 feet	.91	1.40	.107	-1.049	-.654	.575	.145	.243	-.278	.0231	-.0120	-.0891	-.0115	.0745	-.487
34	Sea level	.4	2.60	.142	-.724	-.312	.575	.157	.240	-.240	.0324	-.0078	-.0605	-.0487	.0573	-.372
34	Sea level	.5	1.55	.092	-.756	-.313	.575	.157	.240	-.245	.0209	-.0051	-.0654	-.0344	.0516	-.401
34	Sea level	.6	.90	.064	-.787	-.314	.575	.157	.240	-.251	.0144	-.0036	-.0704	-.0260	.0487	-.430
34	Sea level	.7	.50	.046	-.835	-.322	.575	.157	.240	-.256	.0103	-.0029	-.0757	-.0230	.0458	-.458
34	Sea level	.8	.30	.035	-.918	-.341	.575	.157	.240	-.265	.0077	-.0026	-.0810	-.0171	.0573	-.487
34	Sea level	.85	.2	.030	-.972	-.379	.575	.157	.240	-.269	.0066	-.0025	-.0836	-.0115	.0630	-.516
34	Sea level	.875	.1	.028	-1.005	-.447	.575	.157	.240	-.271	.0061	-.0025	-.0848	-.0056	.0688	-.516
34	Sea level	.9	.05	.026	-1.036	-.565	.575	.157	.240	-.275	.0056	-.0027	-.0869	-.0029	.0716	-.487
34	Sea level	.91	.1	.026	-1.049	-.654	.575	.157	.240	-.278	.0056	-.0029	-.0881	-.0029	.0745	-.487
34	40,000 feet	.6	6.20	.345	-.787	-.314	.575	.157	.240	-.251	.0776	-.0197	-.0759	-.1003	.0620	-.430
34	40,000 feet	.7	4.30	.253	-.835	-.322	.575	.157	.240	-.256	.0564	-.0158	-.0784	-.0688	.0573	-.458
34	40,000 feet	.8	2.85	.195	-.918	-.341	.575	.157	.240	-.265	.0431	-.0143	-.0829	-.0516	.0573	-.487
34	40,000 feet	.85	2.35	.173	-.972	-.379	.575	.157	.240	-.269	.0381	-.0144	-.0848	-.0372	.0630	-.516
34	40,000 feet	.875	2.14	.163	-1.005	-.447	.575	.157	.240	-.271	.0355	-.0148	-.0880	-.0287	.0688	-.516
34	40,000 feet	.9	2.00	.155	-1.036	-.565	.575	.157	.240	-.275	.0336	-.0158	-.0890	-.0201	.0716	-.487
34	40,000 feet	.91	2.00	.151	-1.049	-.654	.575	.157	.240	-.278	.0326	-.0170	-.0902	-.0172	.0745	-.487

TABLE II. COORDINATES OF SYMMETRICAL

AIRFOIL SECTION

[All dimensions in percent of wing chord parallel to plane of symmetry of wing]

Station	Upper- and lower-surface ordinate
0	0
.5871	1.0958
.8803	1.3226
1.4661	1.6687
2.9264	2.2597
5.8297	2.9981
8.7103	3.4923
11.5680	3.8626
17.2154	4.3929
22.7728	4.7516
28.2409	4.9951
33.6203	5.1488
38.9118	5.2322
44.1160	5.2200
49.2336	5.1300
54.2654	4.9088
59.2118	4.5506
64.0736	4.0784
68.9587	3.5320
73.5461	2.9550
78.1583	2.3821
82.6881	1.8395
87.1366	1.3383
91.5043	.8757
95.7921	.4408
100.0000	.0206

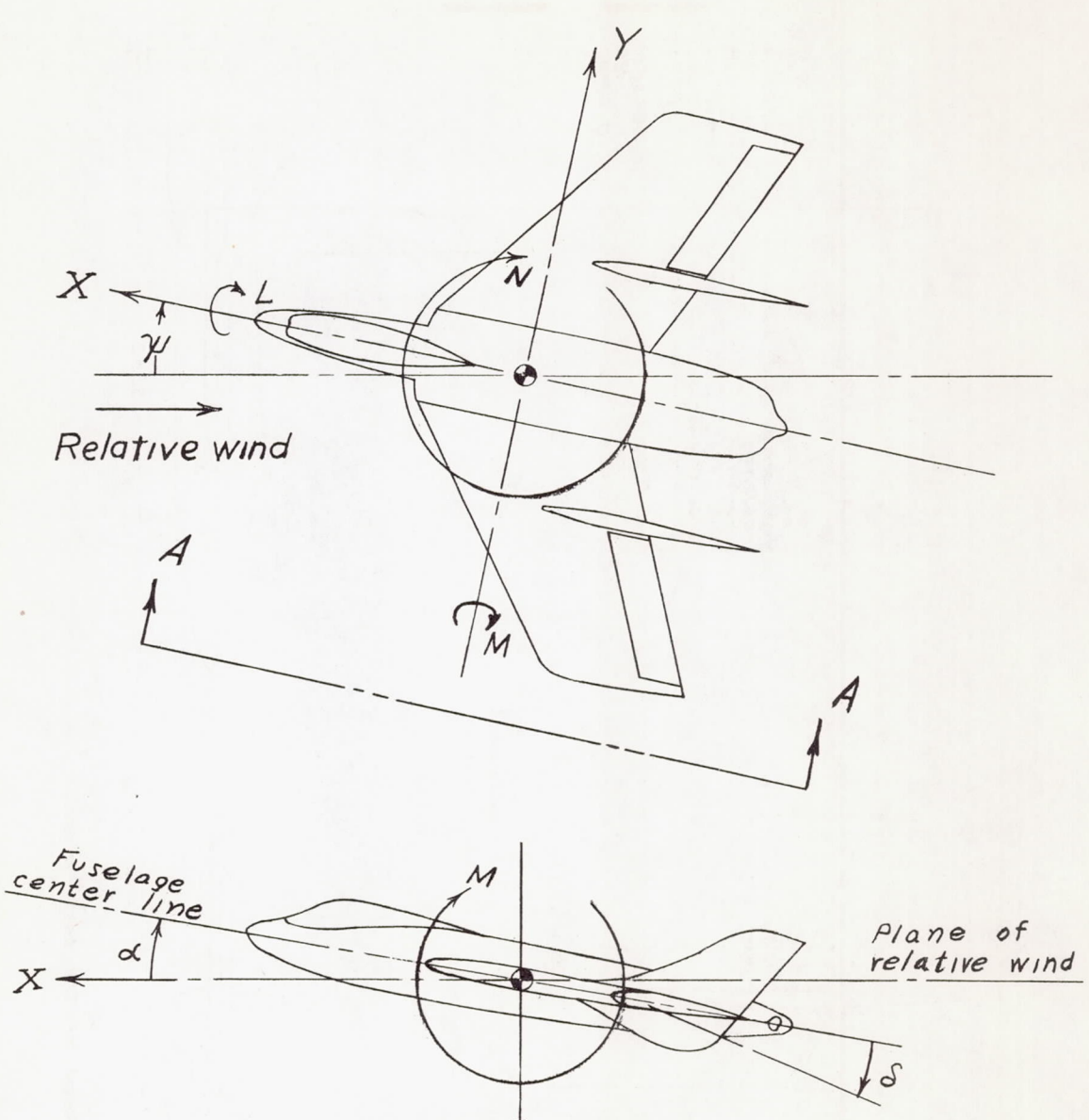

Figure 1.- System of axes and control-surface deflections. Positive values of forces, moments, and angles are indicated by arrows.

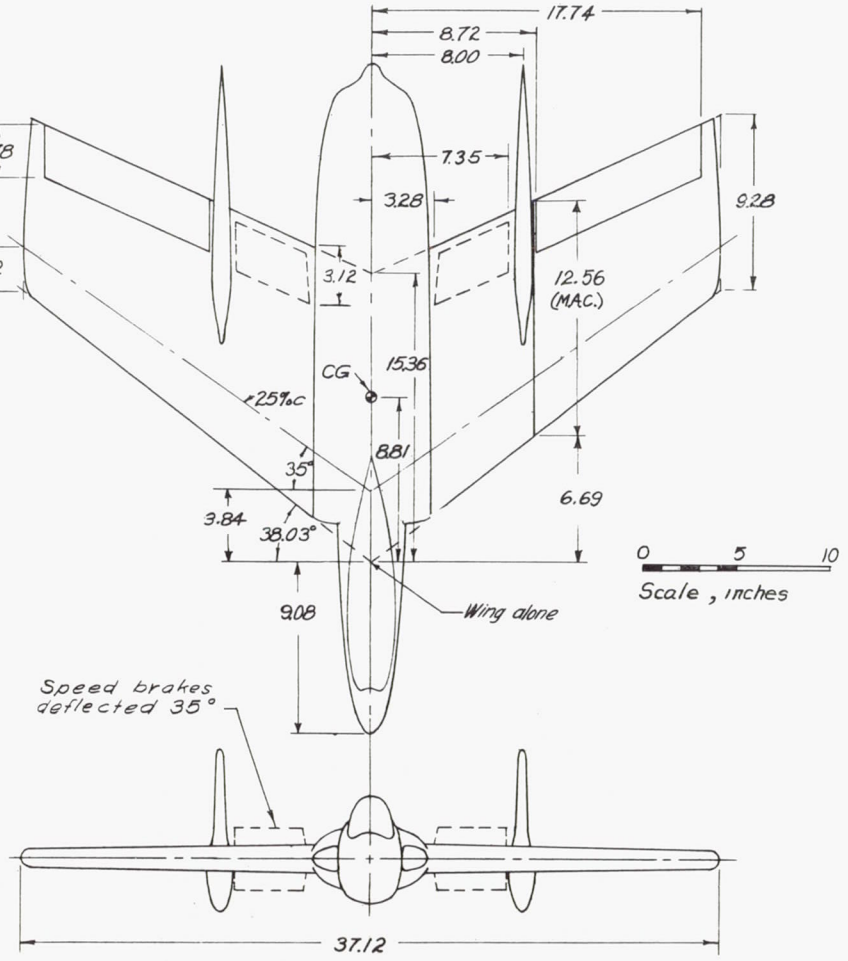

TABULATED DATA

Wing	
Area	3.17 sq ft
Aspect ratio	3.0
Mean aerodynamic chord	1.05 ft
Incidence	0°
Dihedral	0°
Airfoil (Table II)	Symmetrical
Max. thickness	0.105c
Location of max. thickness	0.39c
Vertical tail	
Area (two)	0.82 sq ft
Aspect ratio	1.75
CG location	0.17 M.A.C.

NACA

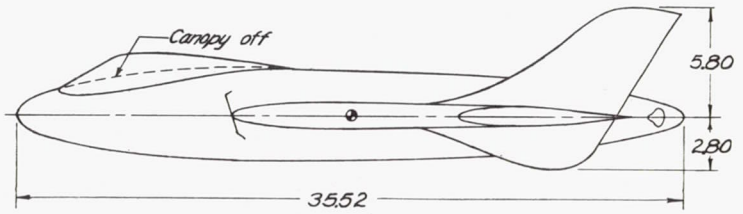

Figure 2.- General arrangement of the test model.

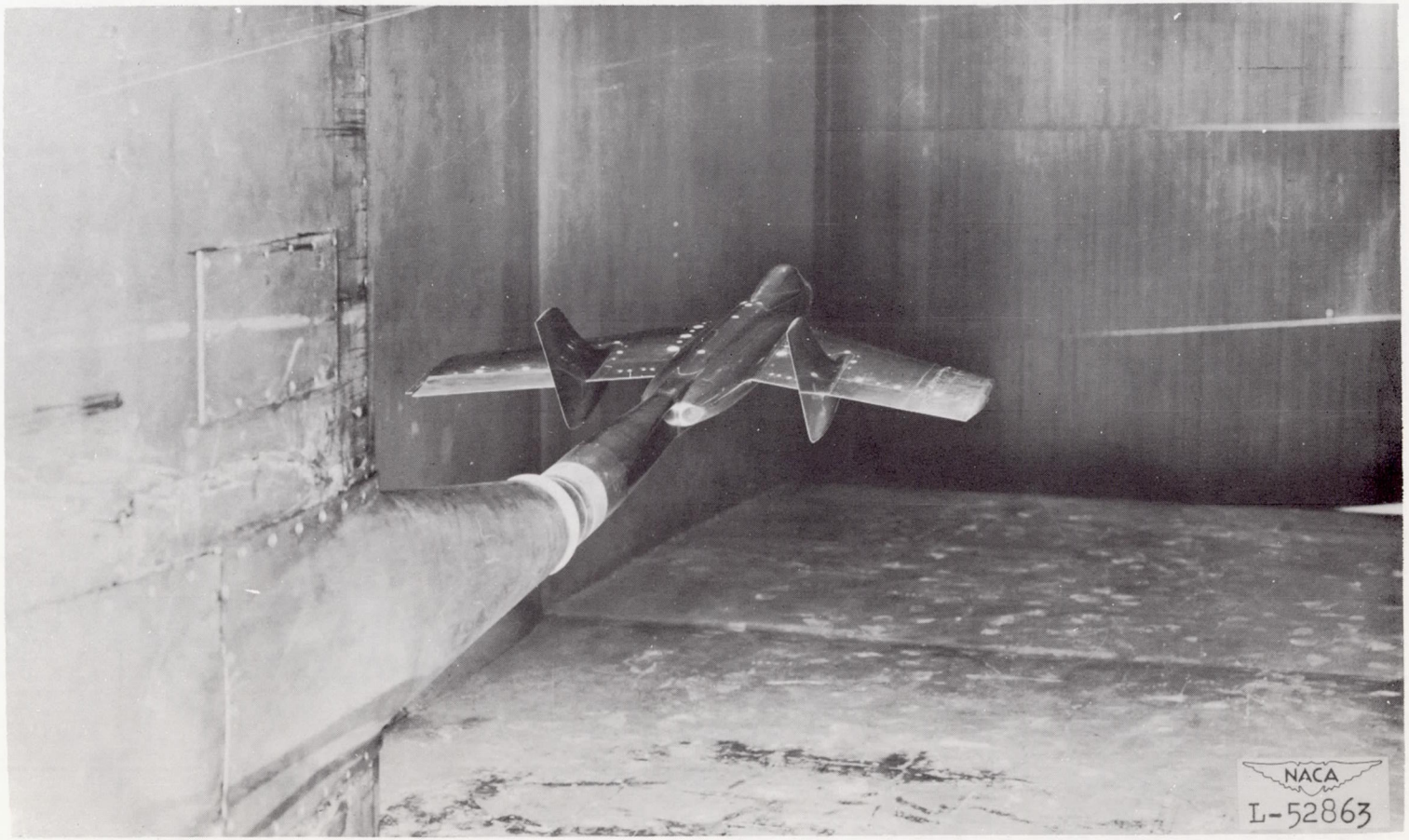

(a) Model mounted on the center sting.

Figure 3.– Photographs of the test model.

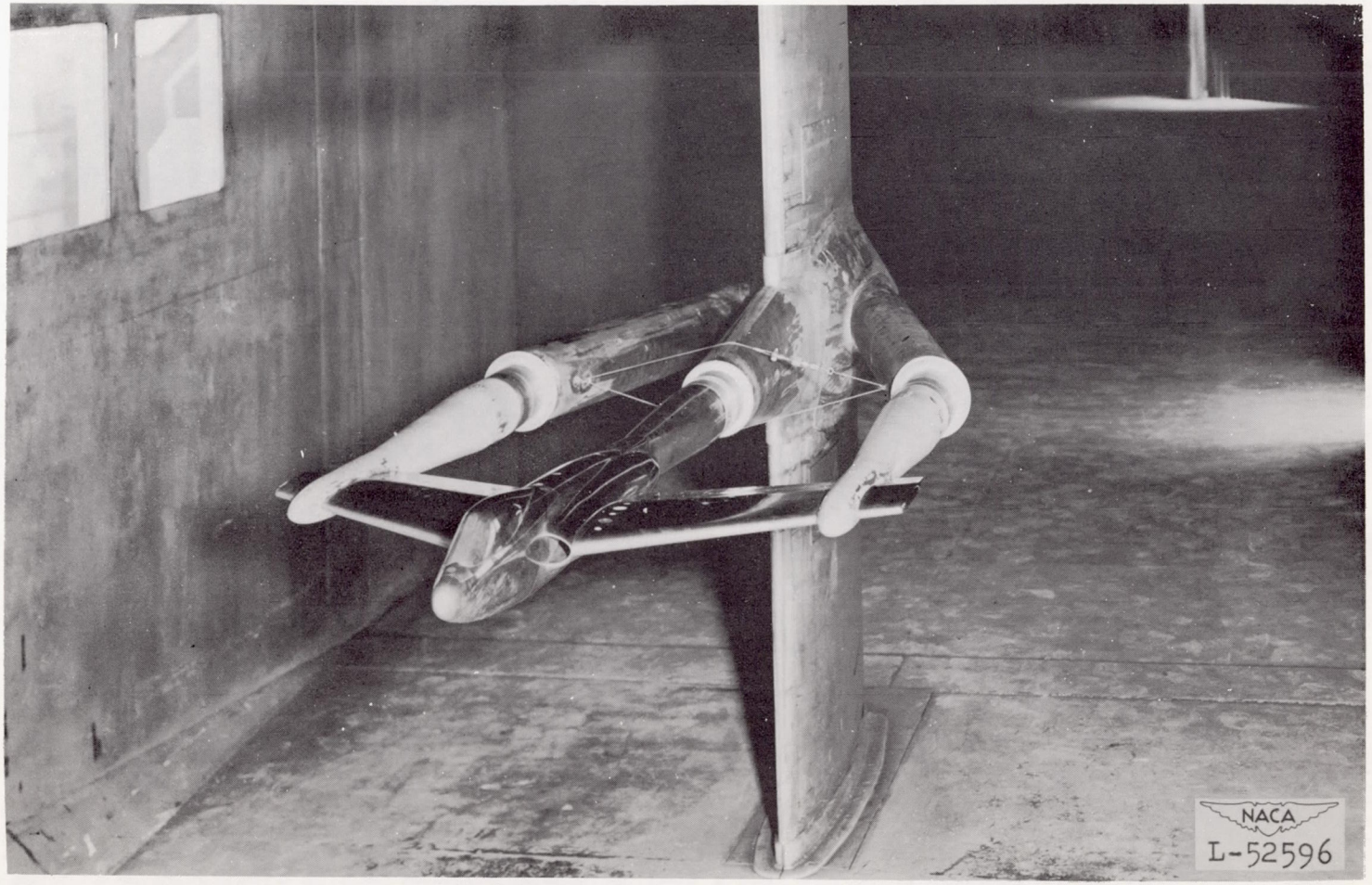

(b) Model mounted on the tare stings with the center sting in place.

Figure 3.- Concluded.

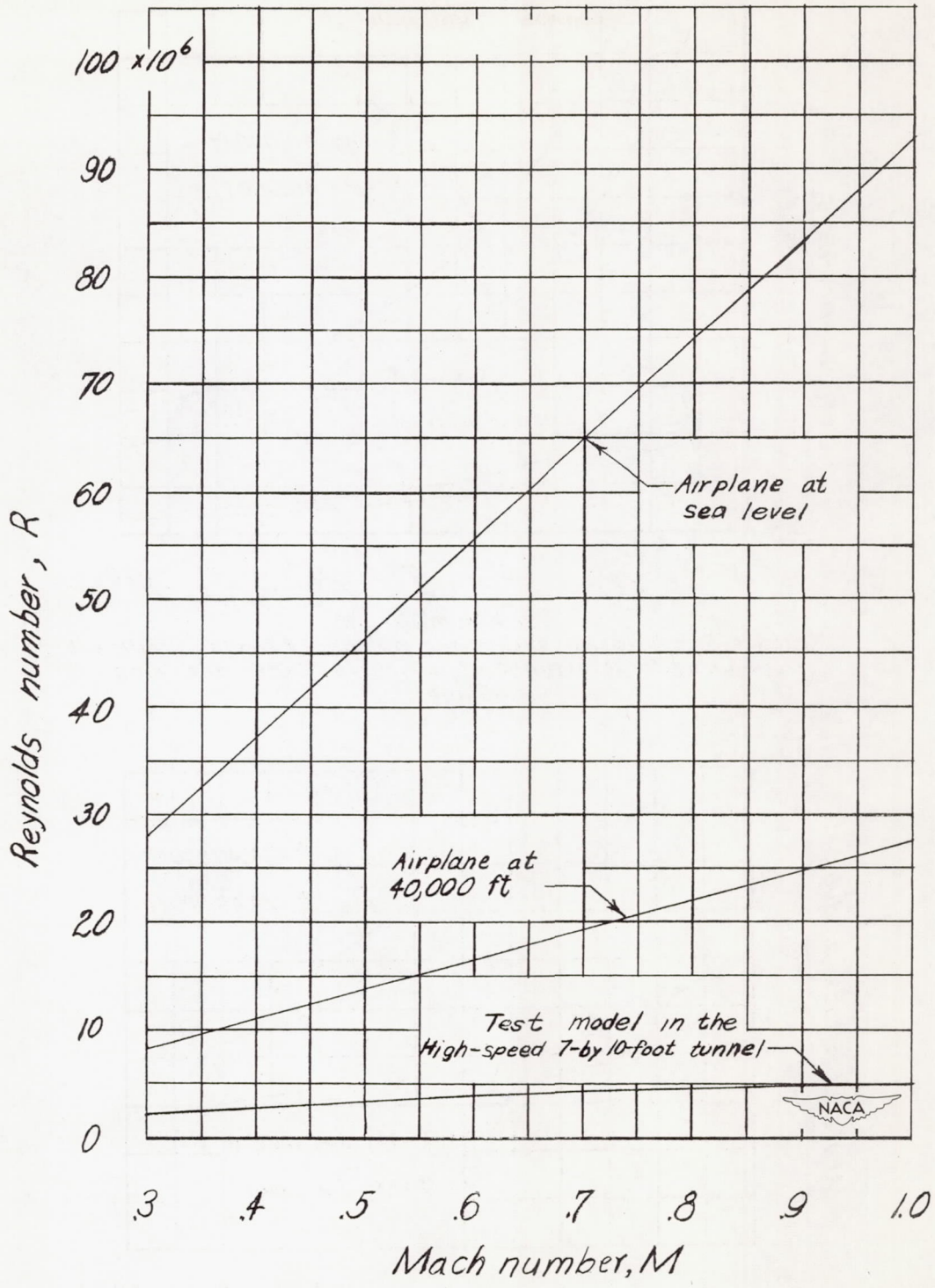

Figure 4.– Variation of Reynolds number with Mach number for flight of the assumed airplane at two altitudes and for wind-tunnel tests data. Based on the model M.A.C. of 1.046 feet and an airplane M.A.C. of 13 feet.

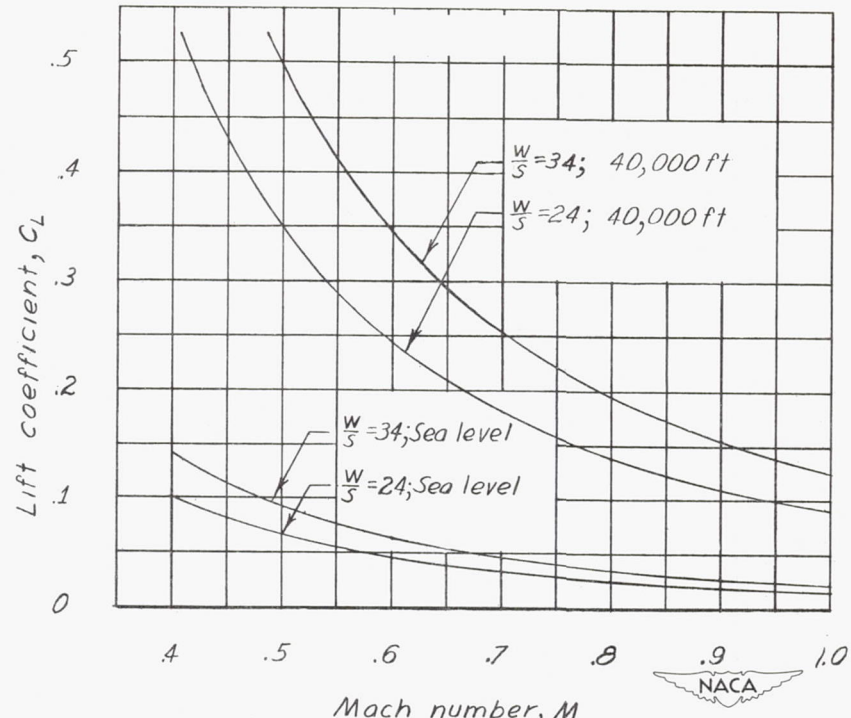

Figure 5.- Variation with Mach number of the lift coefficient required for level flight at various altitudes and wing loadings.

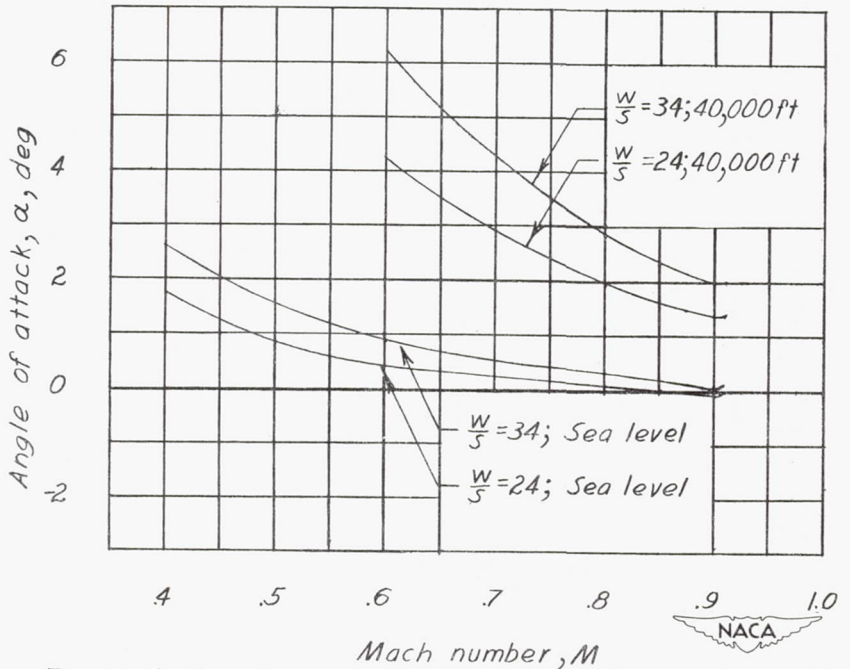

Figure 6.- Variation with Mach number of the angle of attack required for level flight at various altitudes and wing loadings.

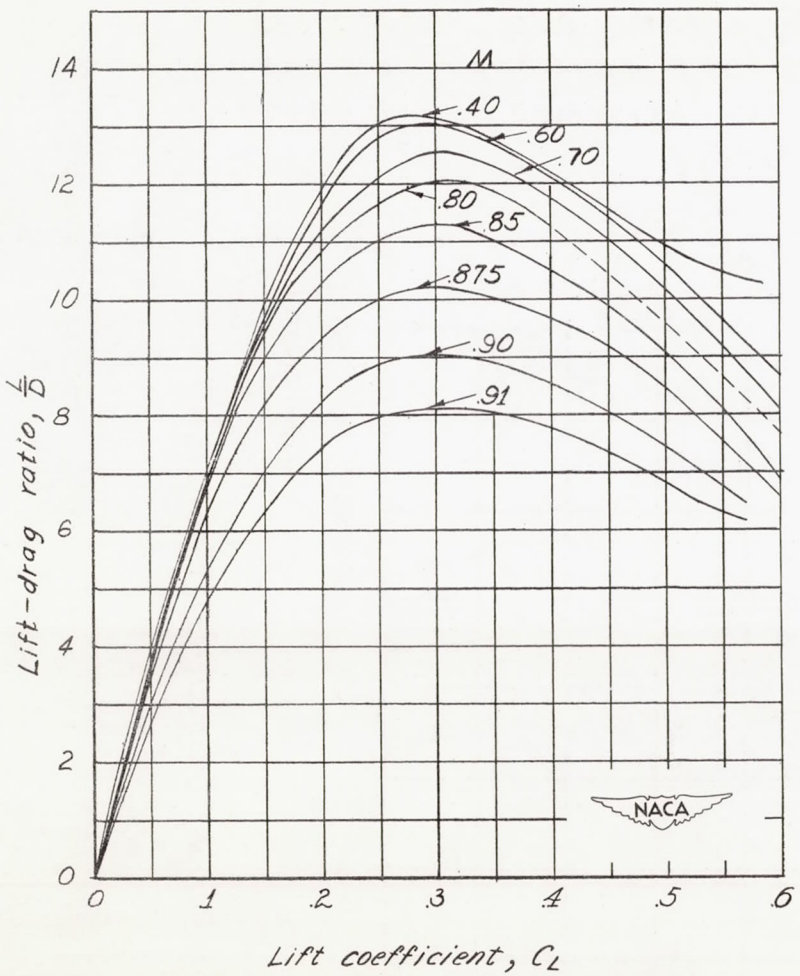

Figure 7.- Variation with lift coefficient of the lift-drag ratio at various Mach numbers. $\delta_a = 0°$.

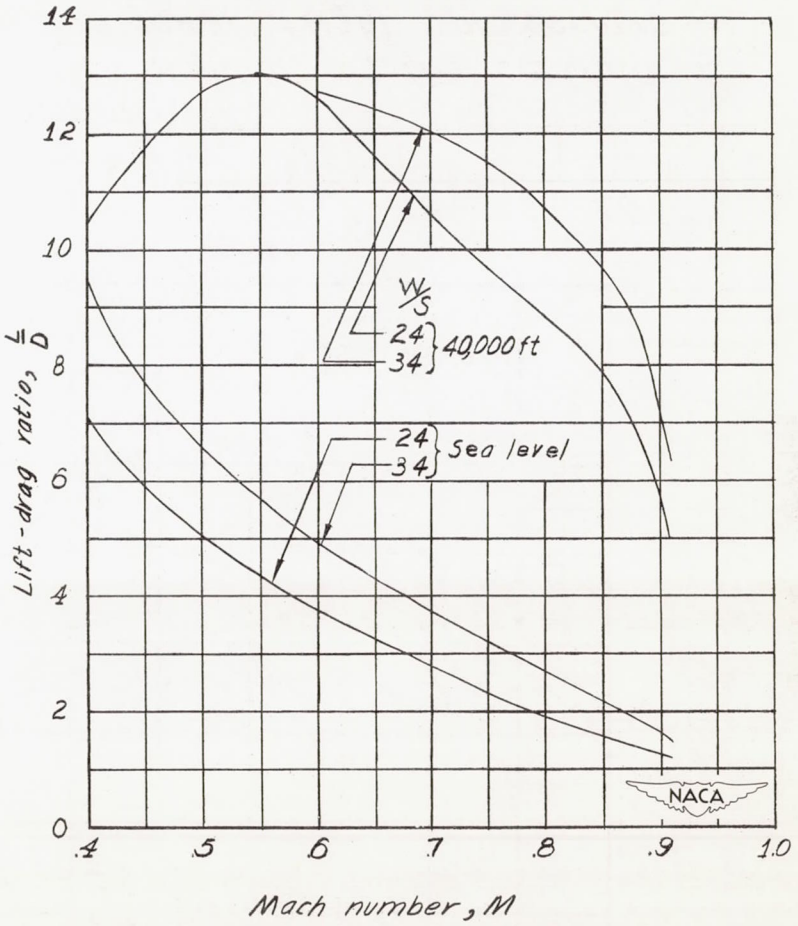

Figure 8.- Variation with Mach number of the lift-drag ratio in level flight at various altitudes and wing loadings. (Trimmed.)

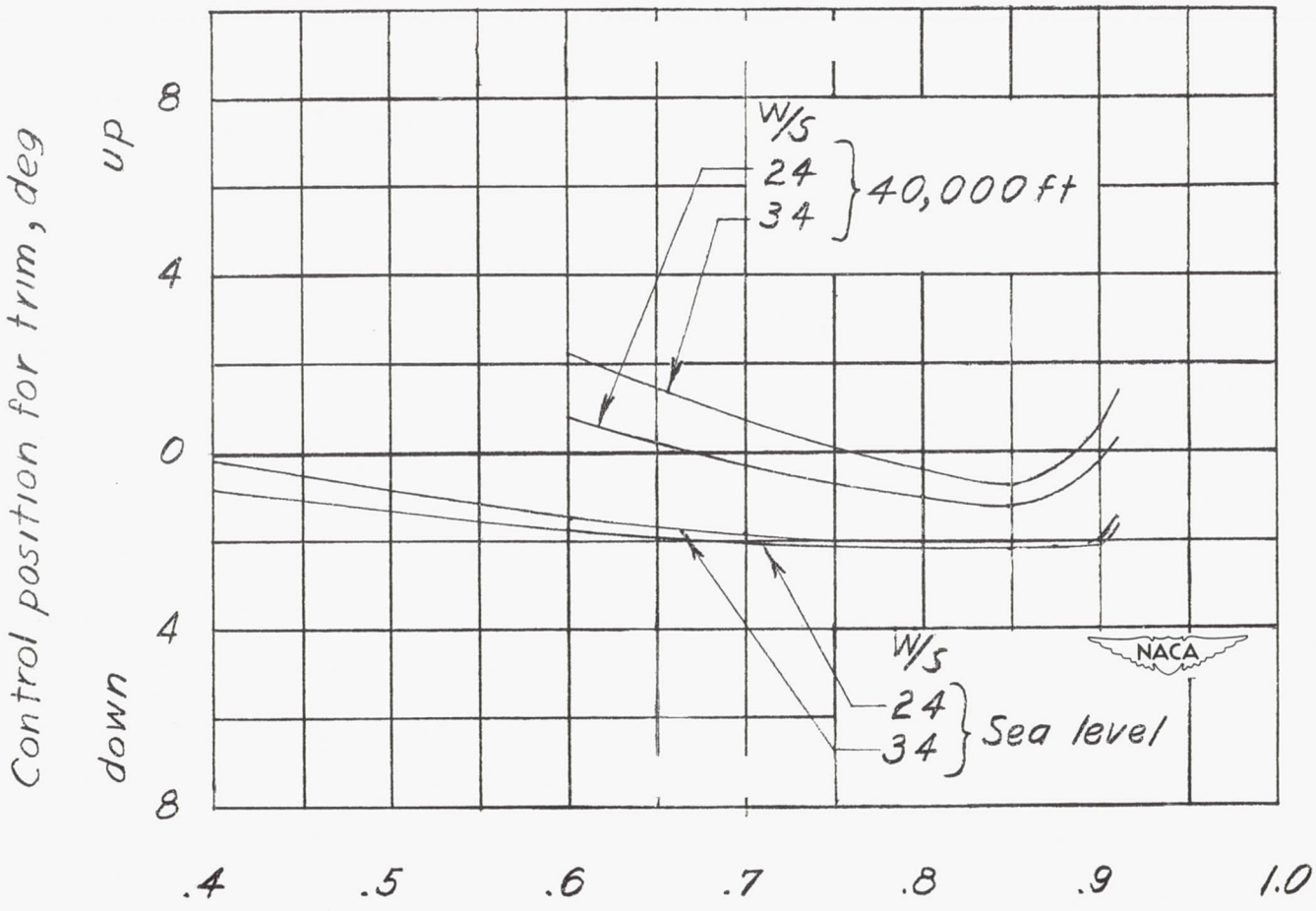

Figure 9.- Variation with Mach number of the control position required for trim in level flight at various altitudes and wing loadings.

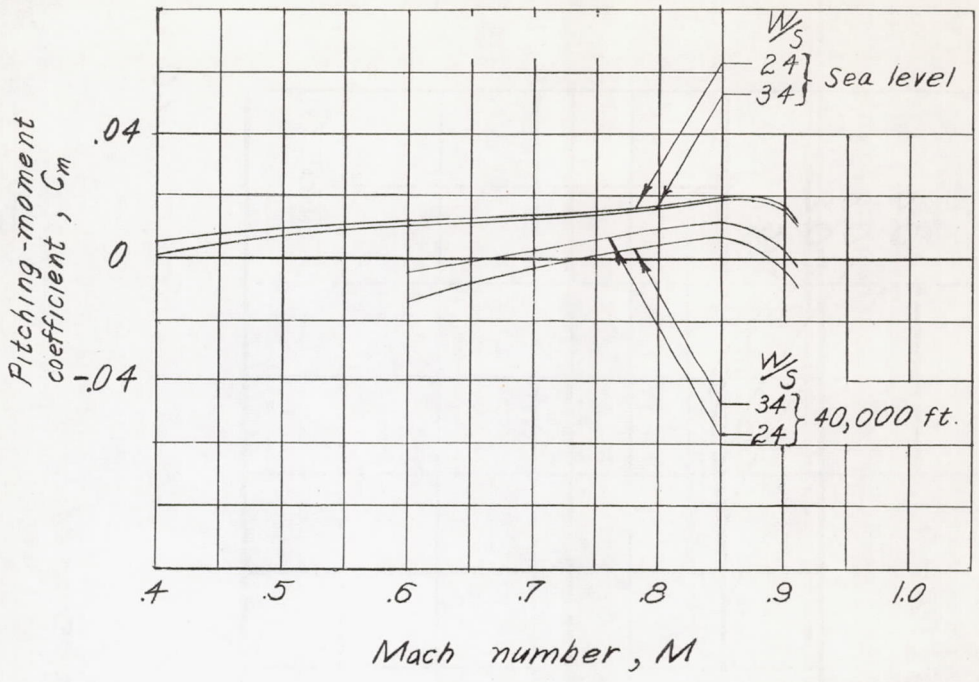

(a) Variation with Mach number of the out-of-trim pitching moment of the model with zero control deflection.

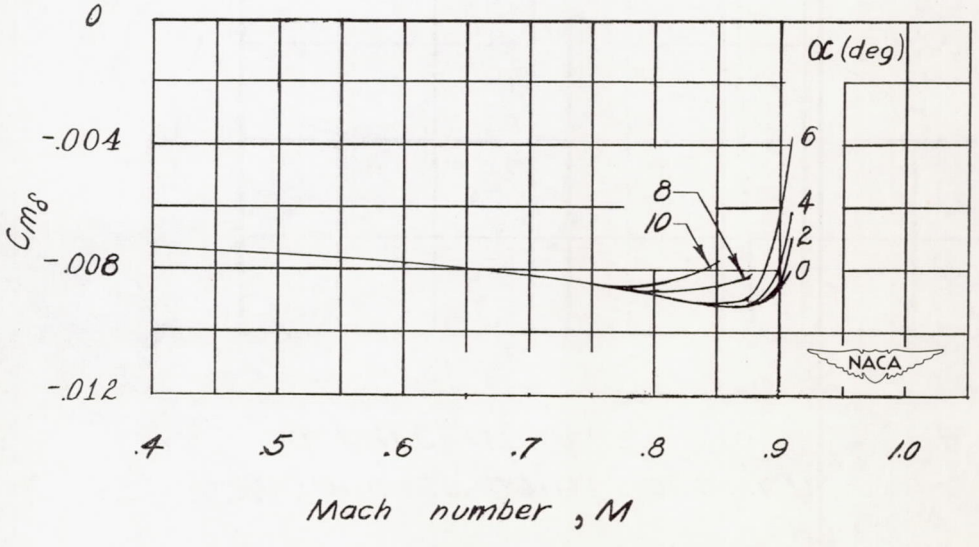

(b) Variation of the control-effectiveness parameter (C_{m_δ}) with Mach number.

Figure 10.— Variation of the out-of-trim pitching moment and the control effectiveness with Mach number.

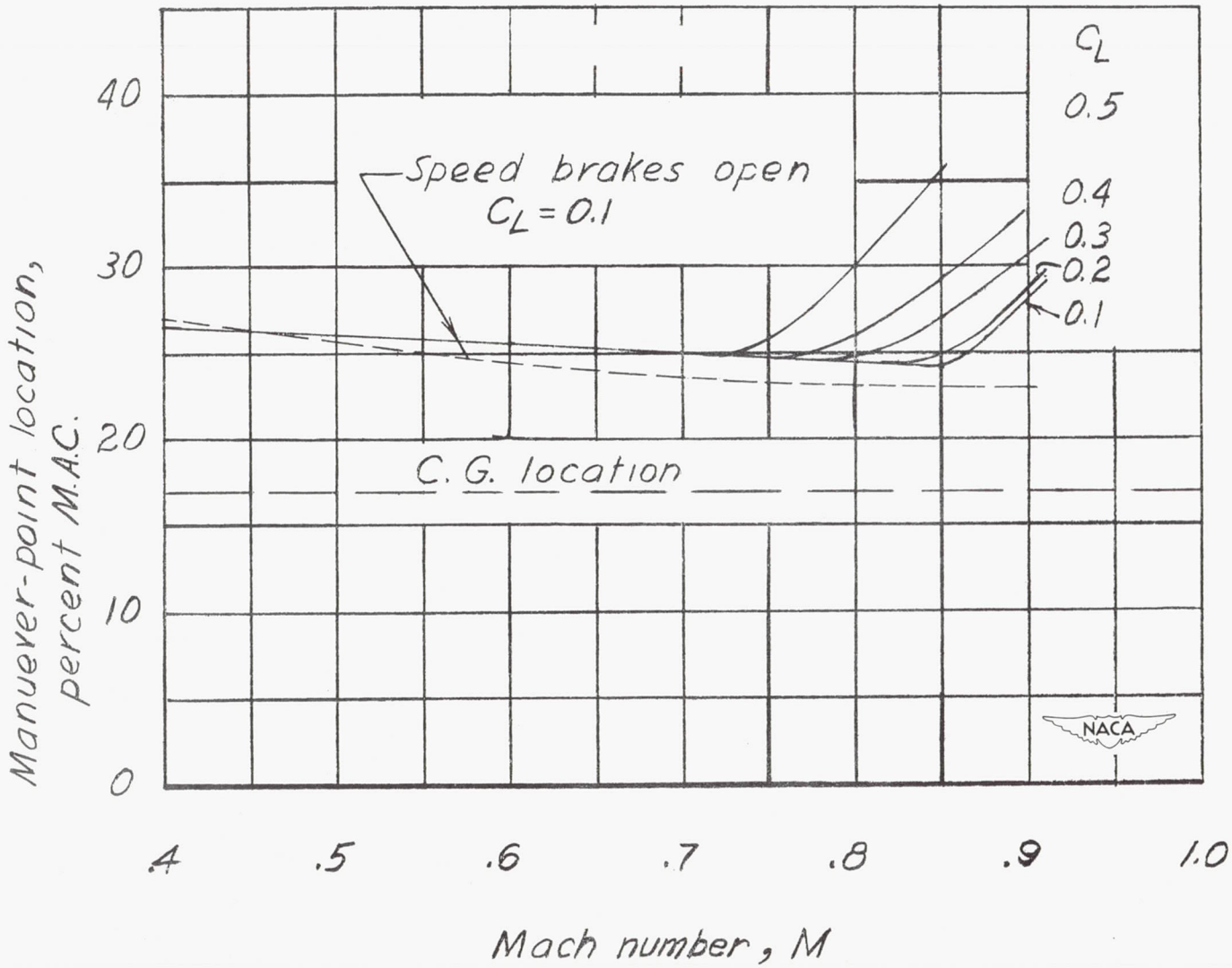

Figure 11.- Variation with Mach number of the maneuver-point location.

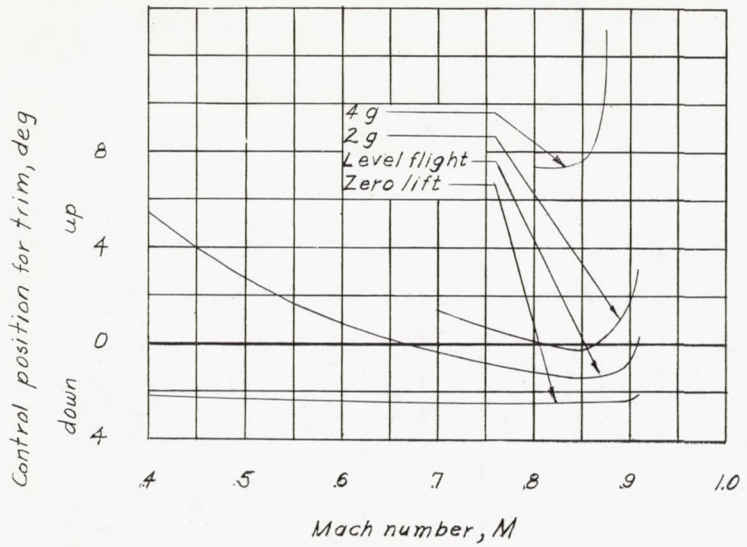

(a) 40,000 ft., $\frac{W}{S}$ = 24.

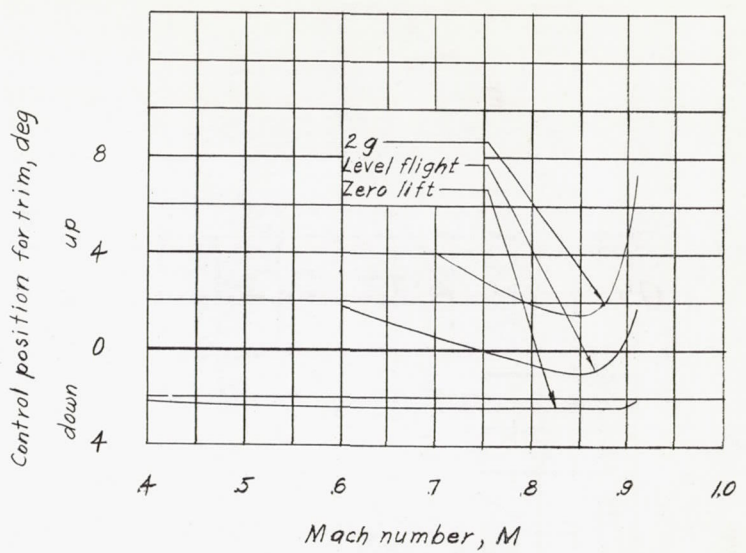

(b) 40,000 ft., $\frac{W}{S}$ = 34.

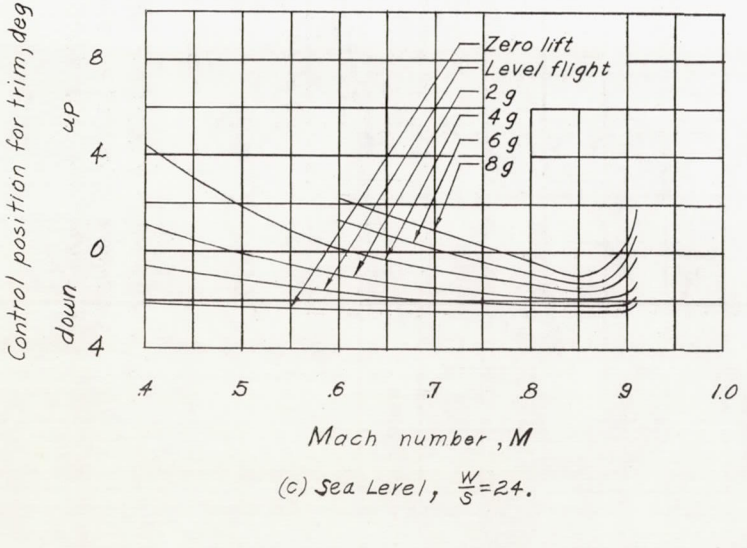

(c) Sea Level, $\frac{W}{S}$ = 24.

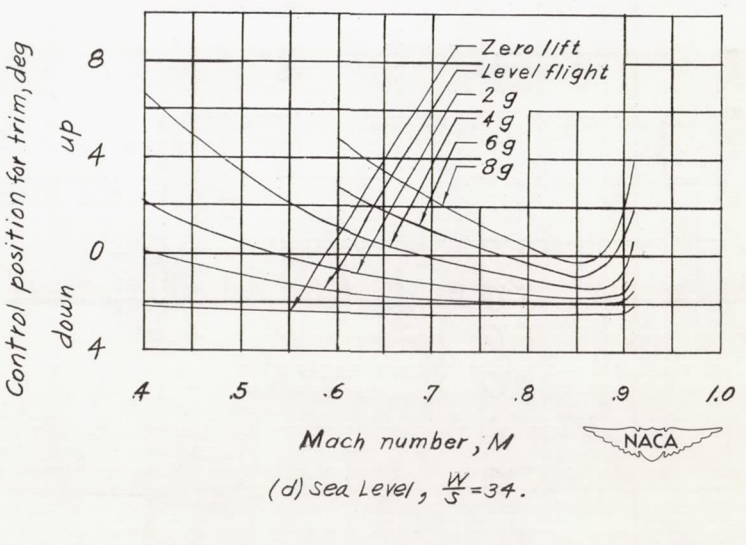

(d) Sea Level, $\frac{W}{S}$ = 34.

Figure 12.- Variation with Mach number of the control position required for trim in level and accelerated flight at various altitudes and wing loadings.

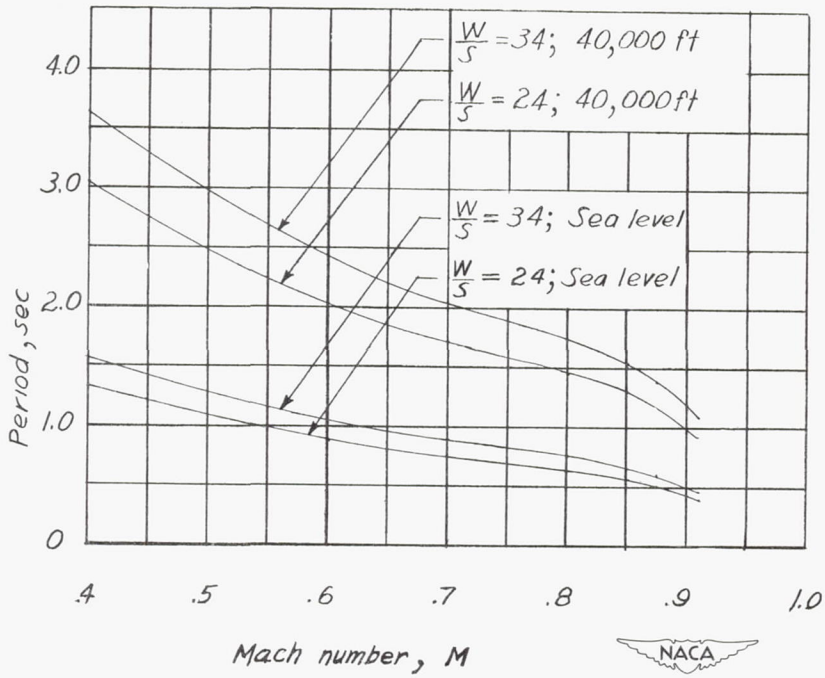

Figure 13.- Variation with Mach number of the period of the short-period longitudinal oscillation.

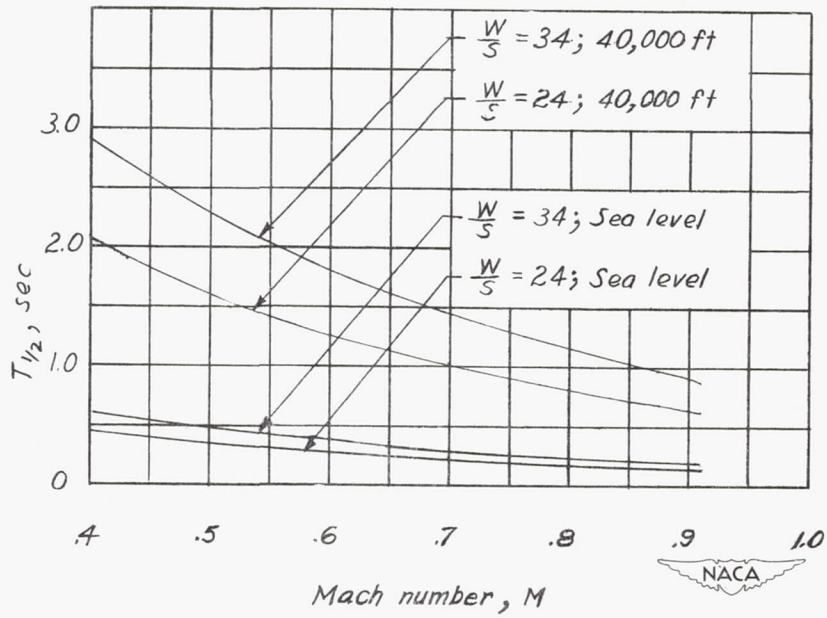

Figure 14.- Variation with Mach number of the time required for the short-period longitudinal oscillation to damp to one-half amplitude.

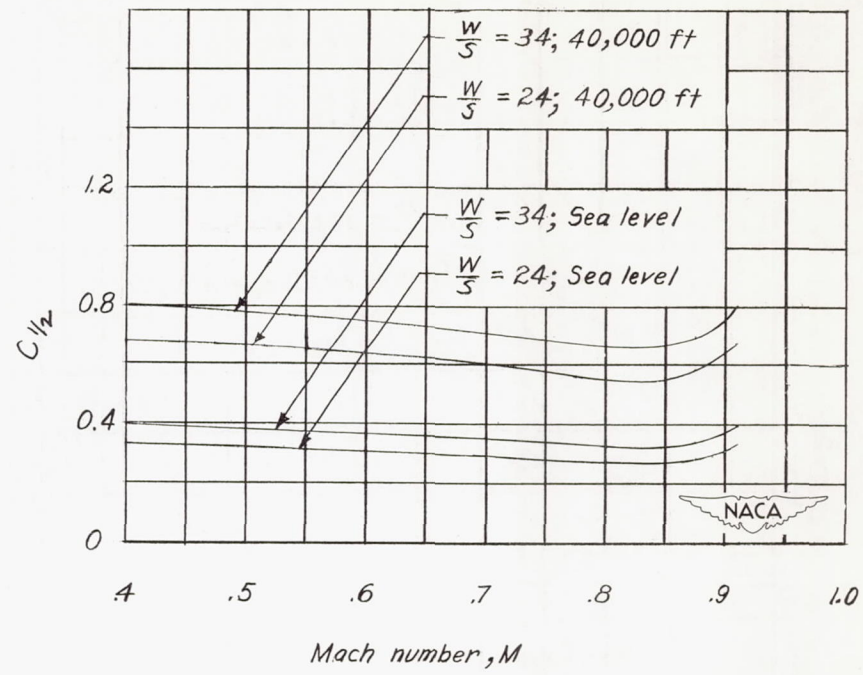

Figure 15.- Variation with Mach number of the number of cycles required for the short-period longitudinal oscillation to damp to one-half amplitude.

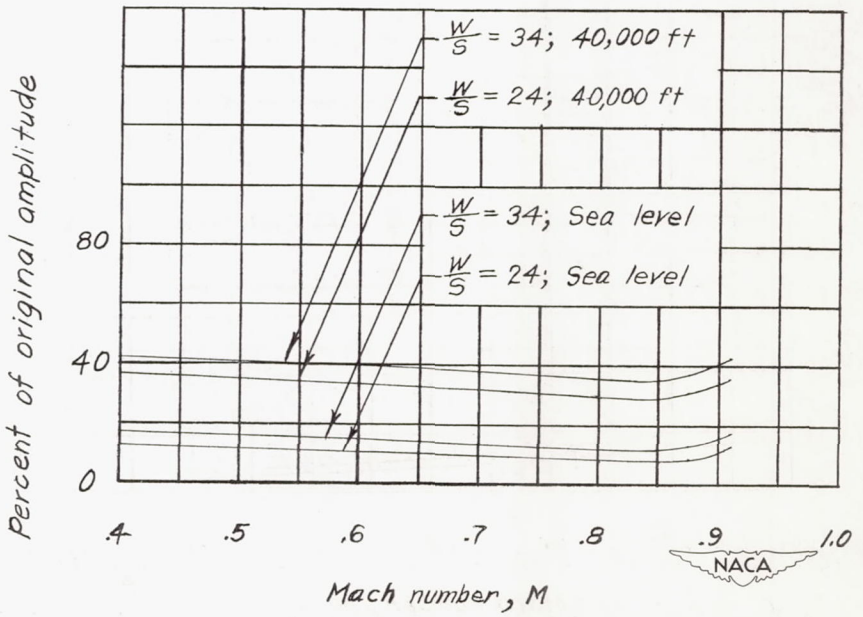

Figure 16.- Variation with Mach number of the amplitude of the short-period longitudinal oscillation after one cycle in percent of the original amplitude.

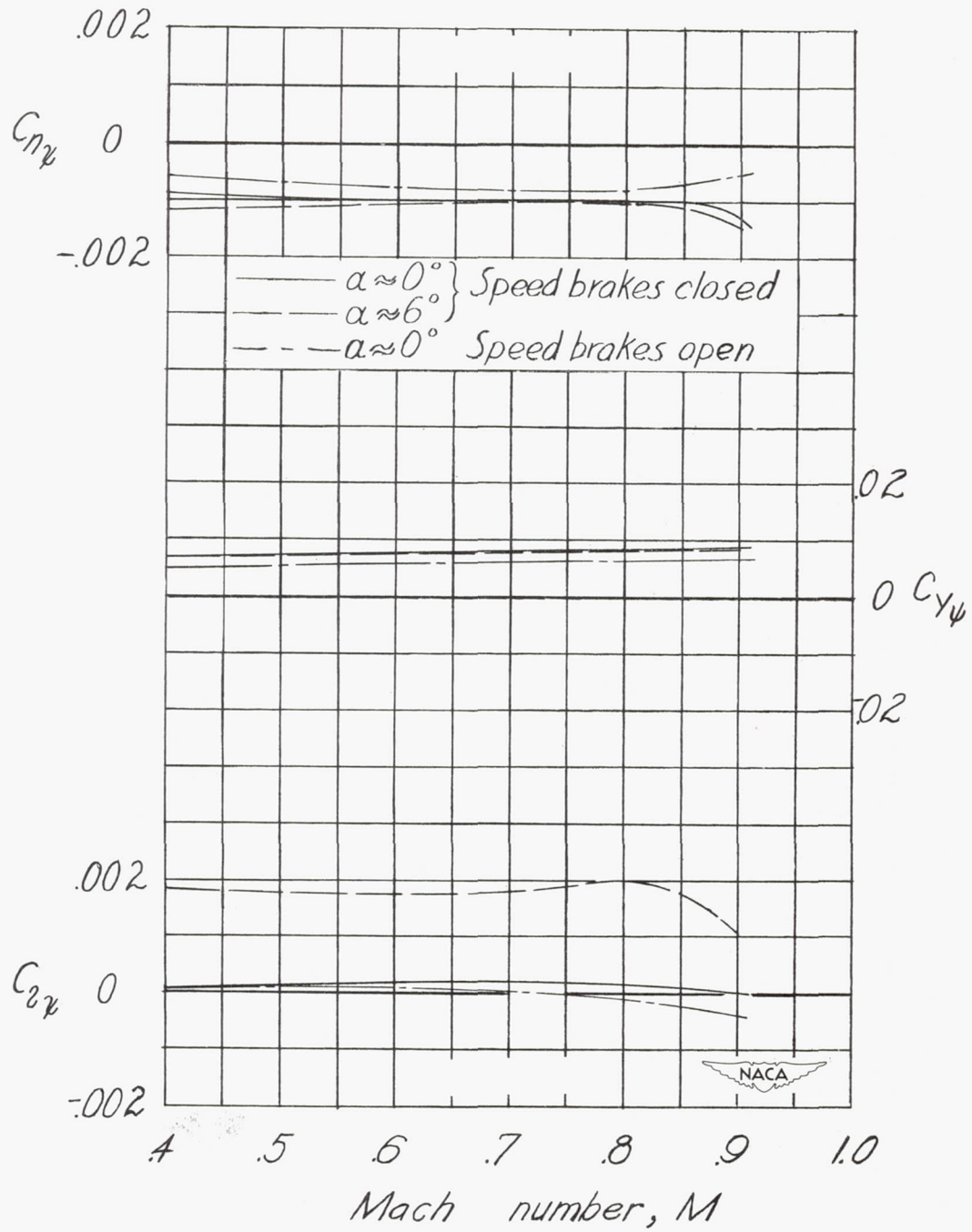

Figure 17.- Variation with Mach number of the lateral stability characteristics of the test model.

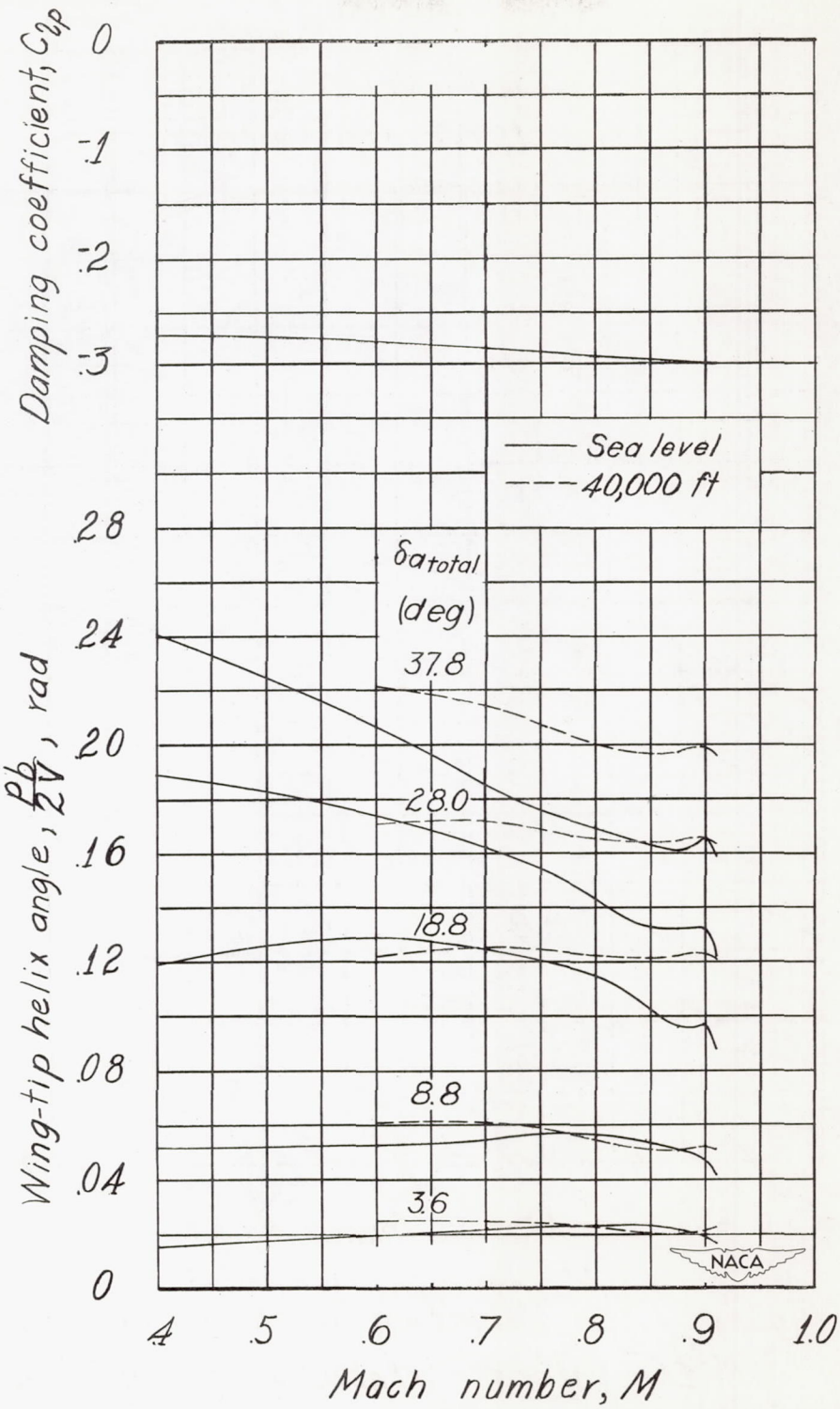

Figure 18.- Variation of the wing-tip helix angle with Mach number for various total aileron deflections.

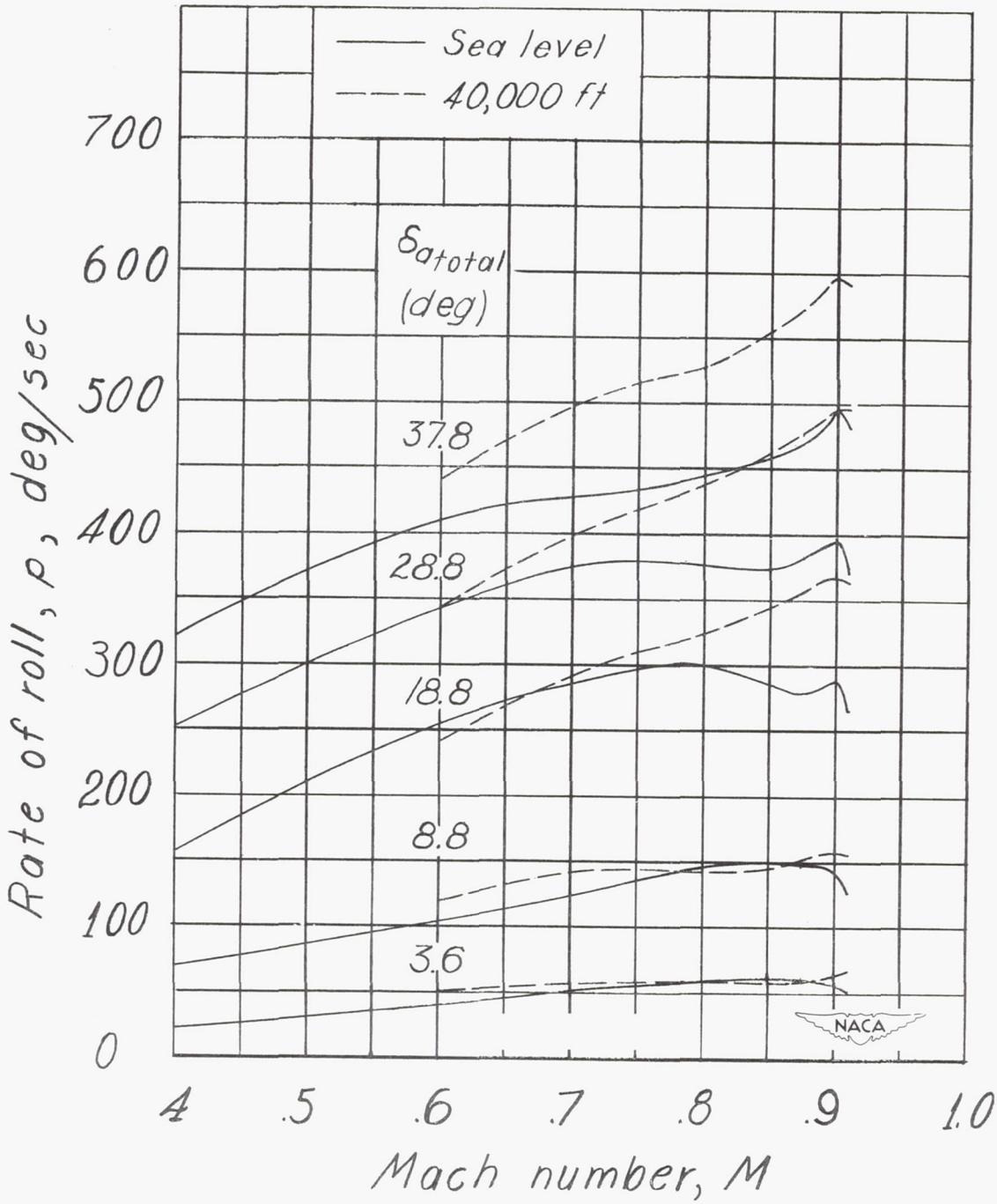

Figure 19.- Variation with Mach number of the rate of roll for various total aileron deflections.

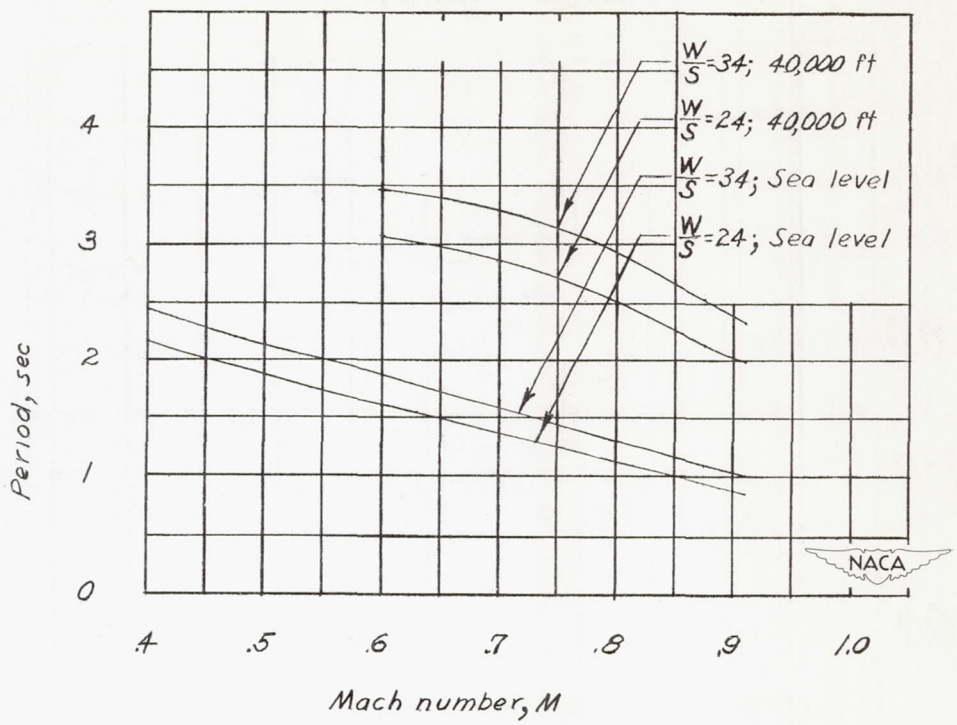

Figure 20.- Variation with Mach number of the period of the lateral oscillation.

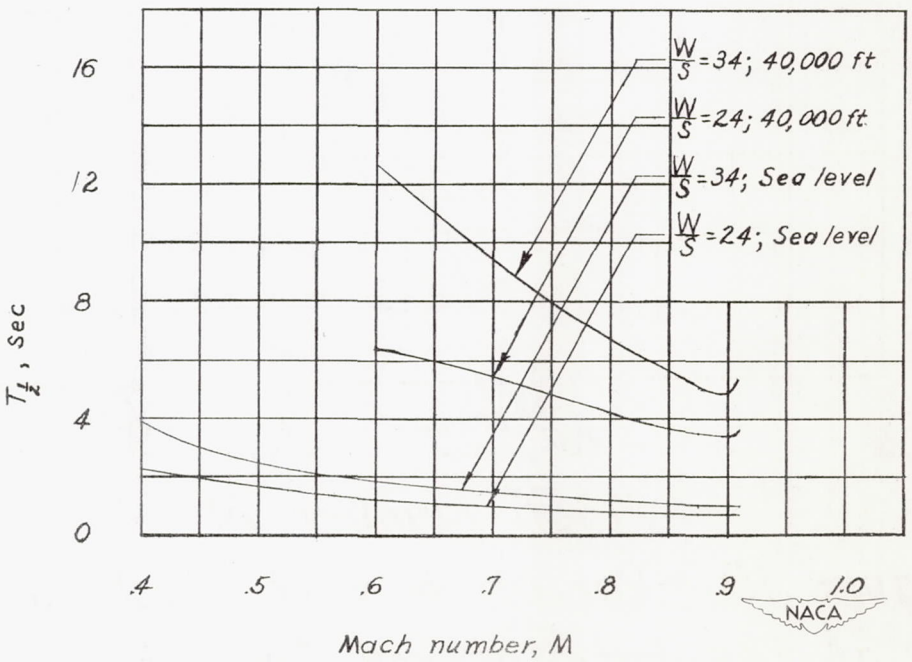

Figure 21.- Variation with Mach number of the time required for the lateral oscillation to damp to one-half amplitude.

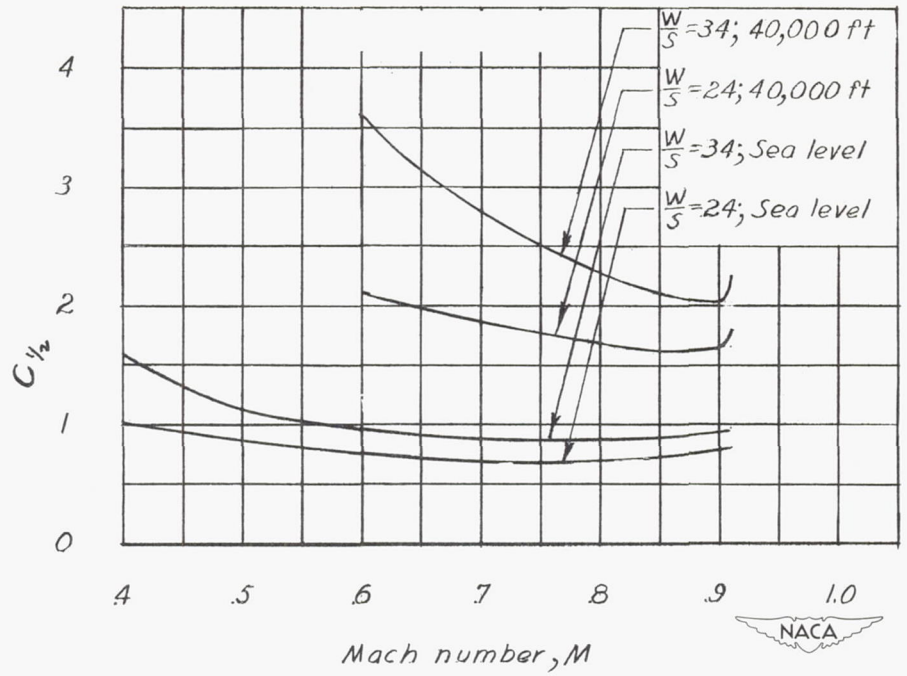

Figure 22.- Variation with Mach number of the number of cycles required for the lateral oscillation to damp to one-half amplitude.

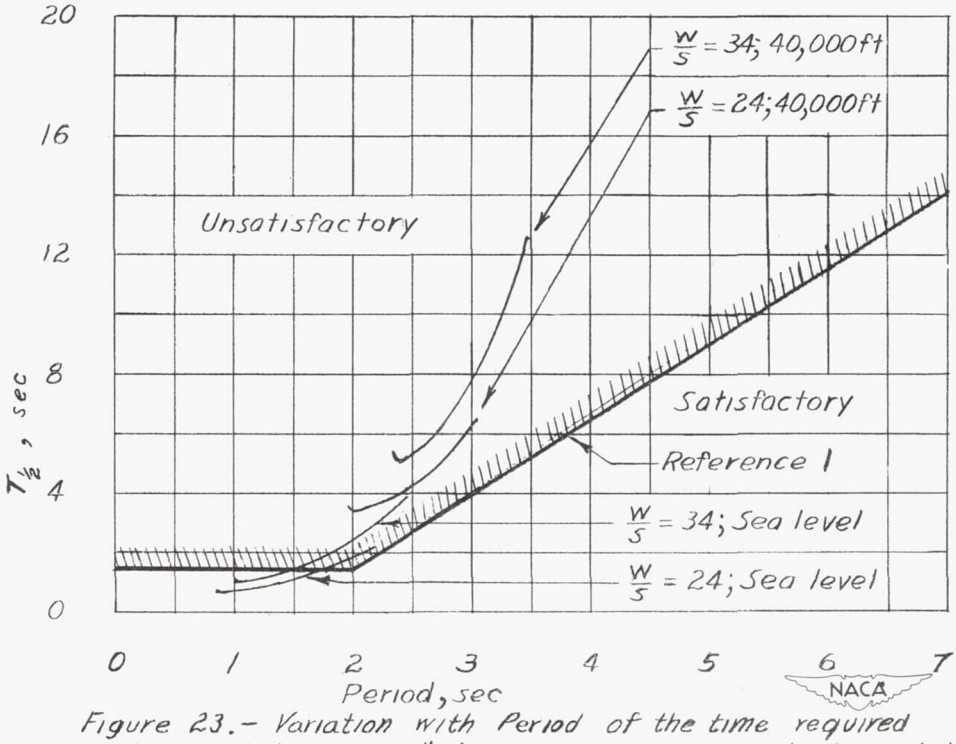

Figure 23.- Variation with Period of the time required for the lateral oscillation to damp to one-half amplitude.

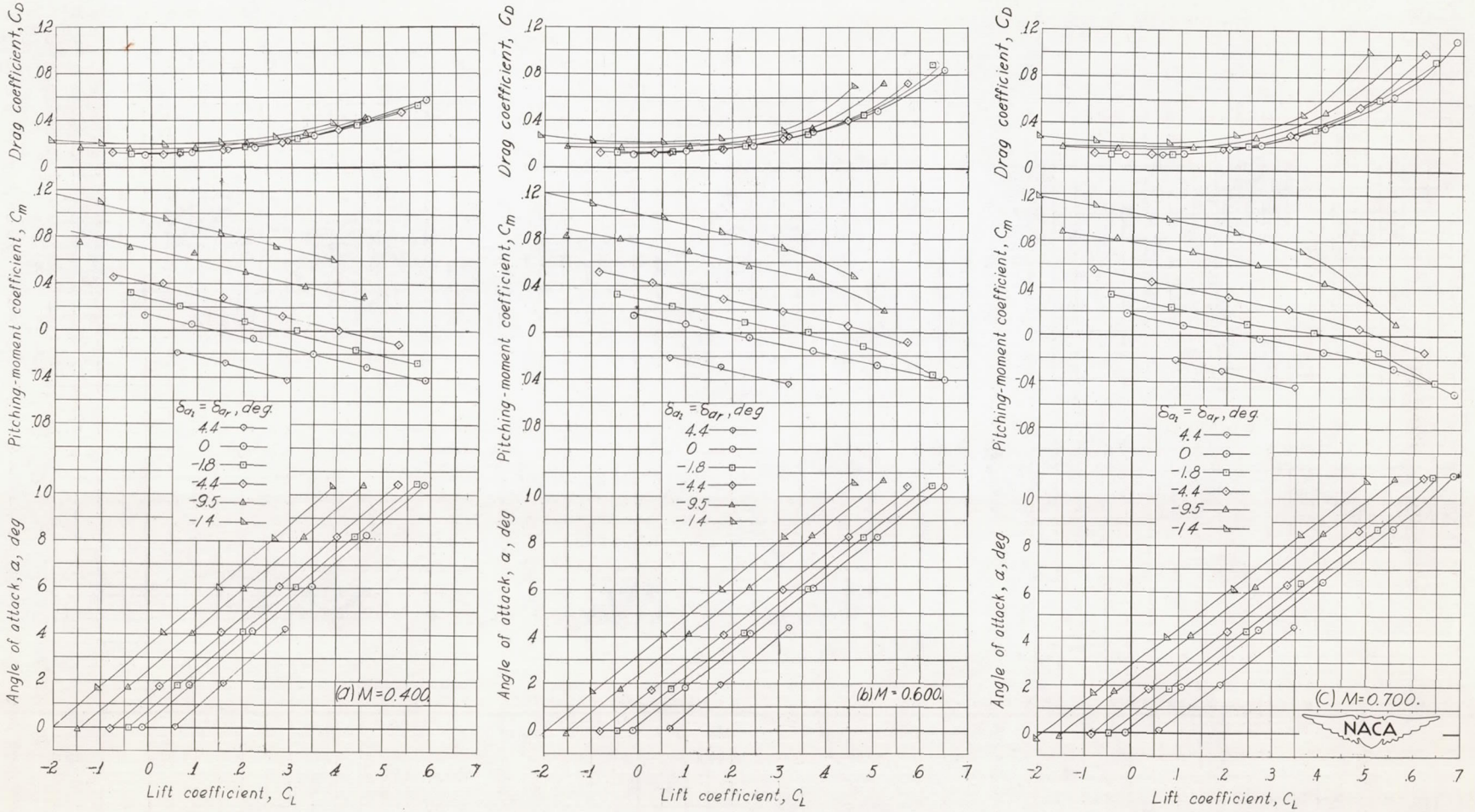

Figure 24.-Effect of control deflection on the aerodynamic characteristics in pitch of the test model.

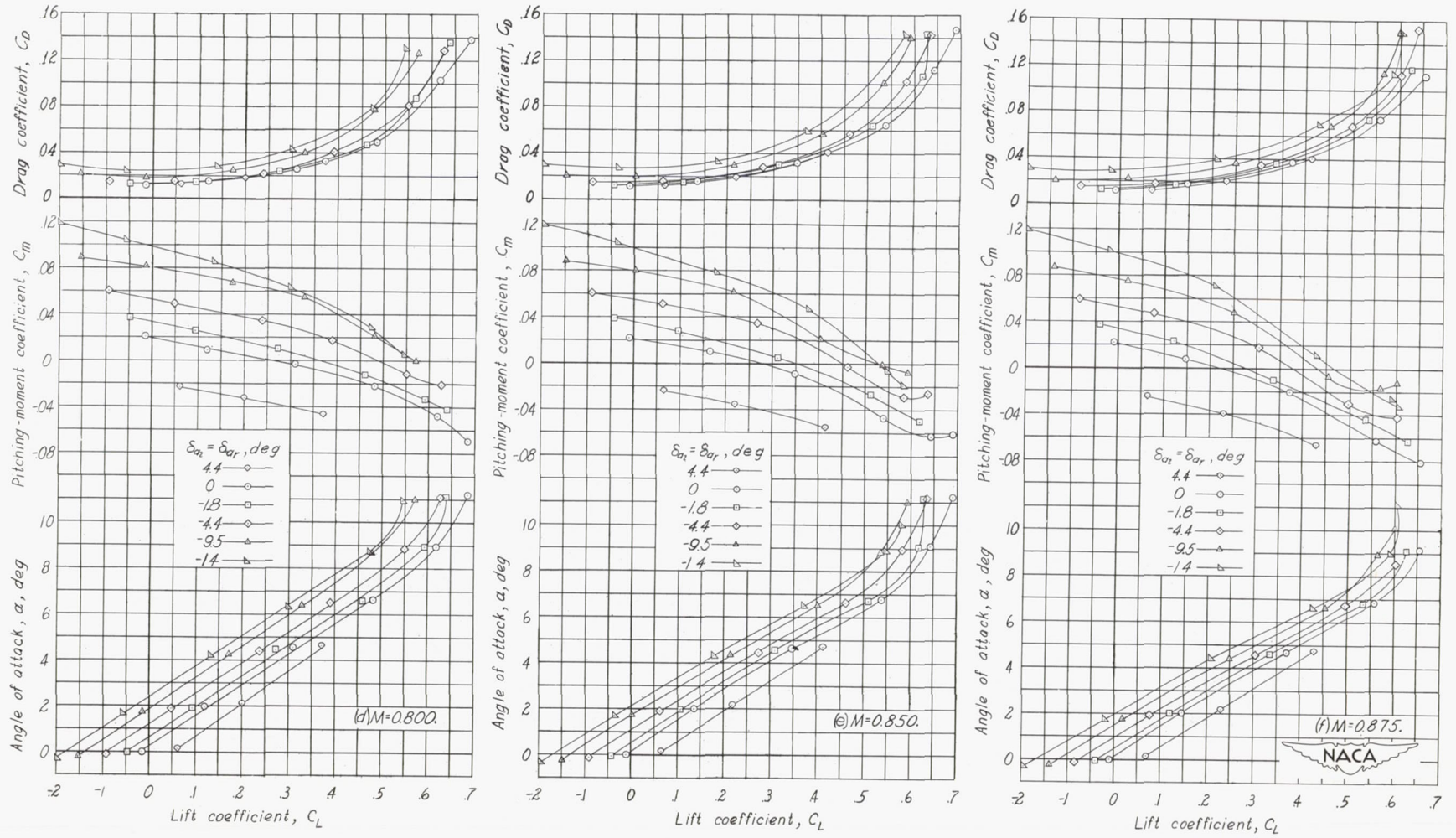

Figure 24.—Continued.

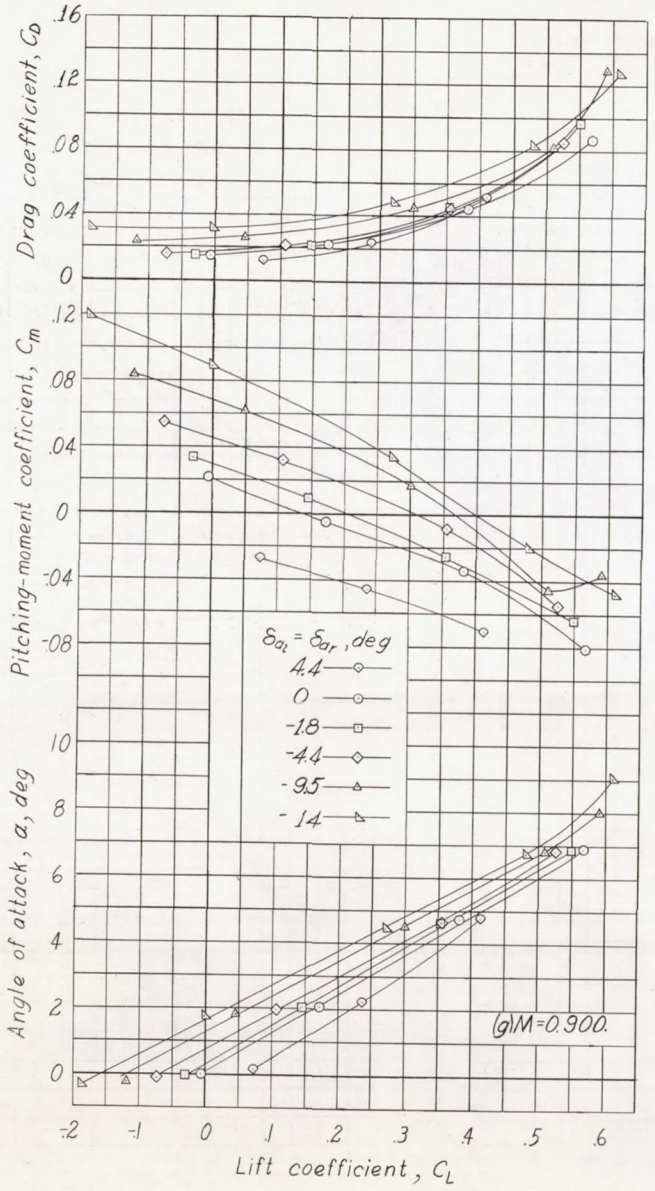

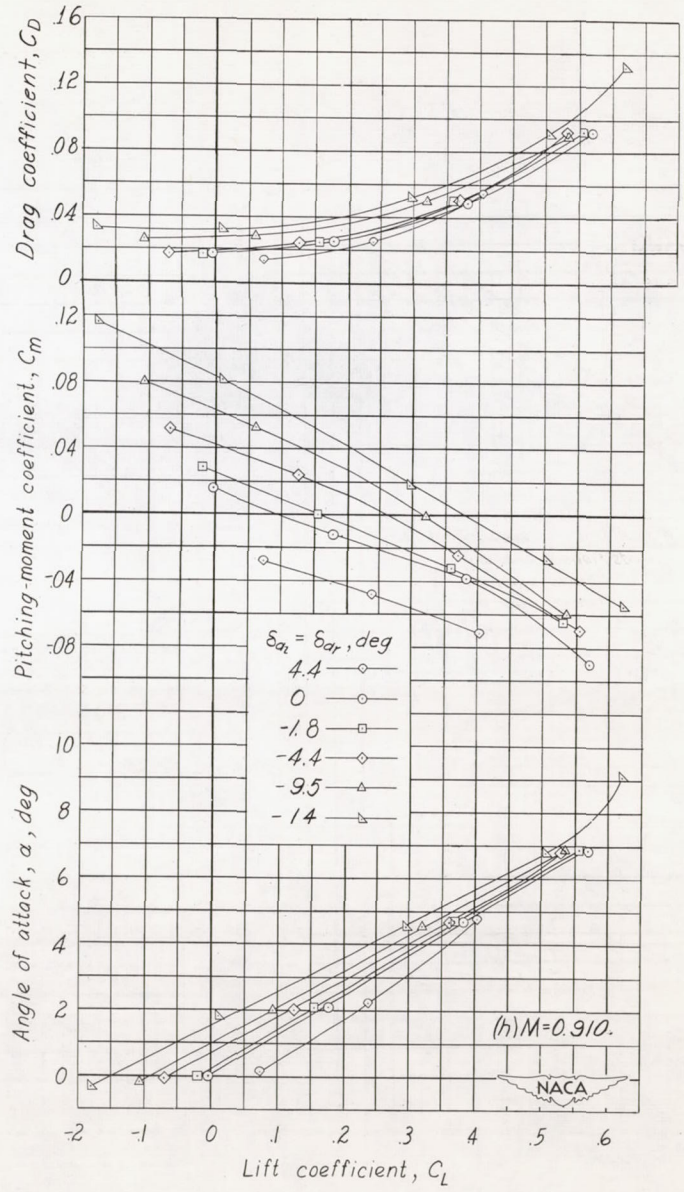

Figure 24.-Concluded.

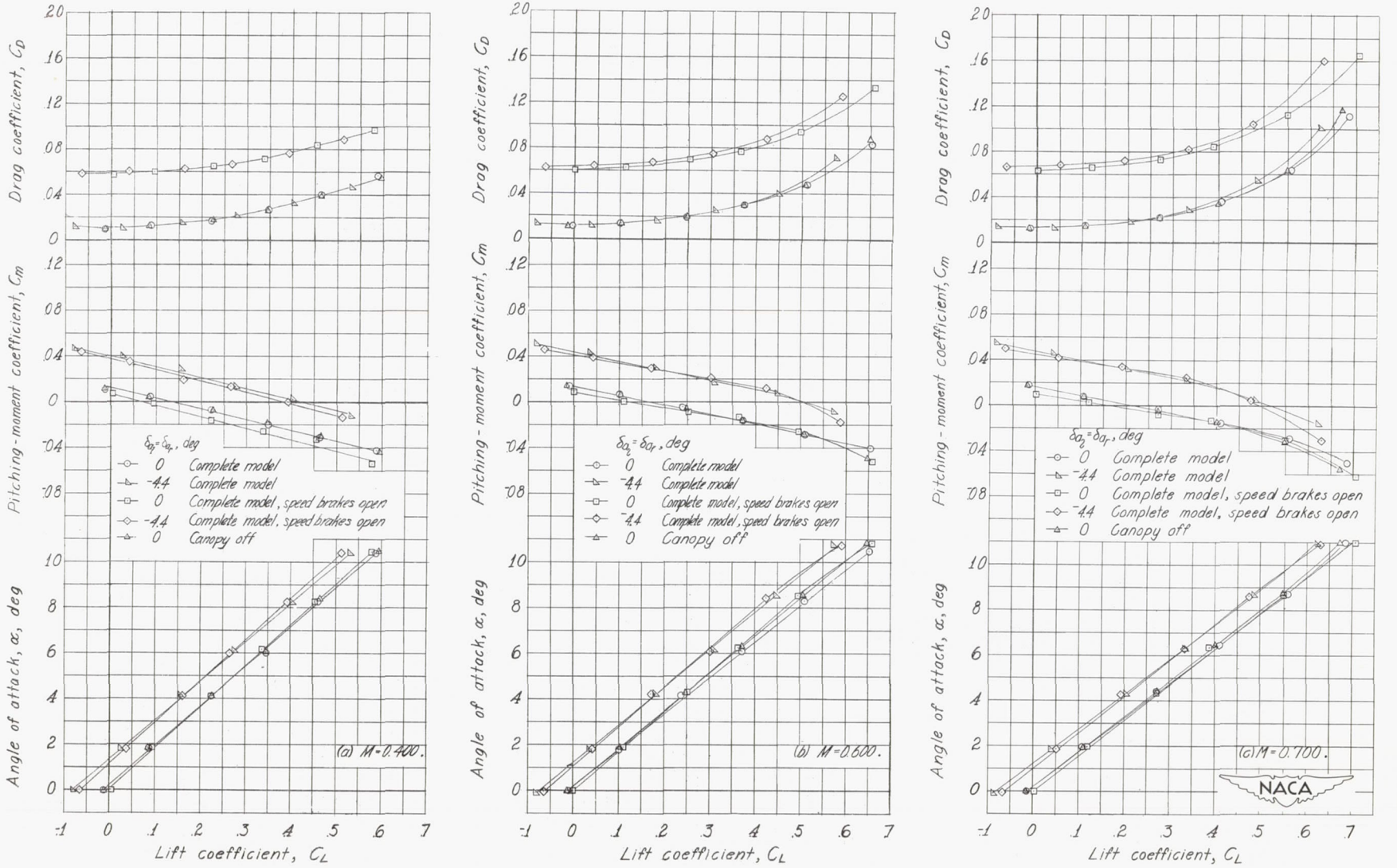

Figure 25. - Effect of speed brakes and canopy on the aerodynamic characteristics of the test model.

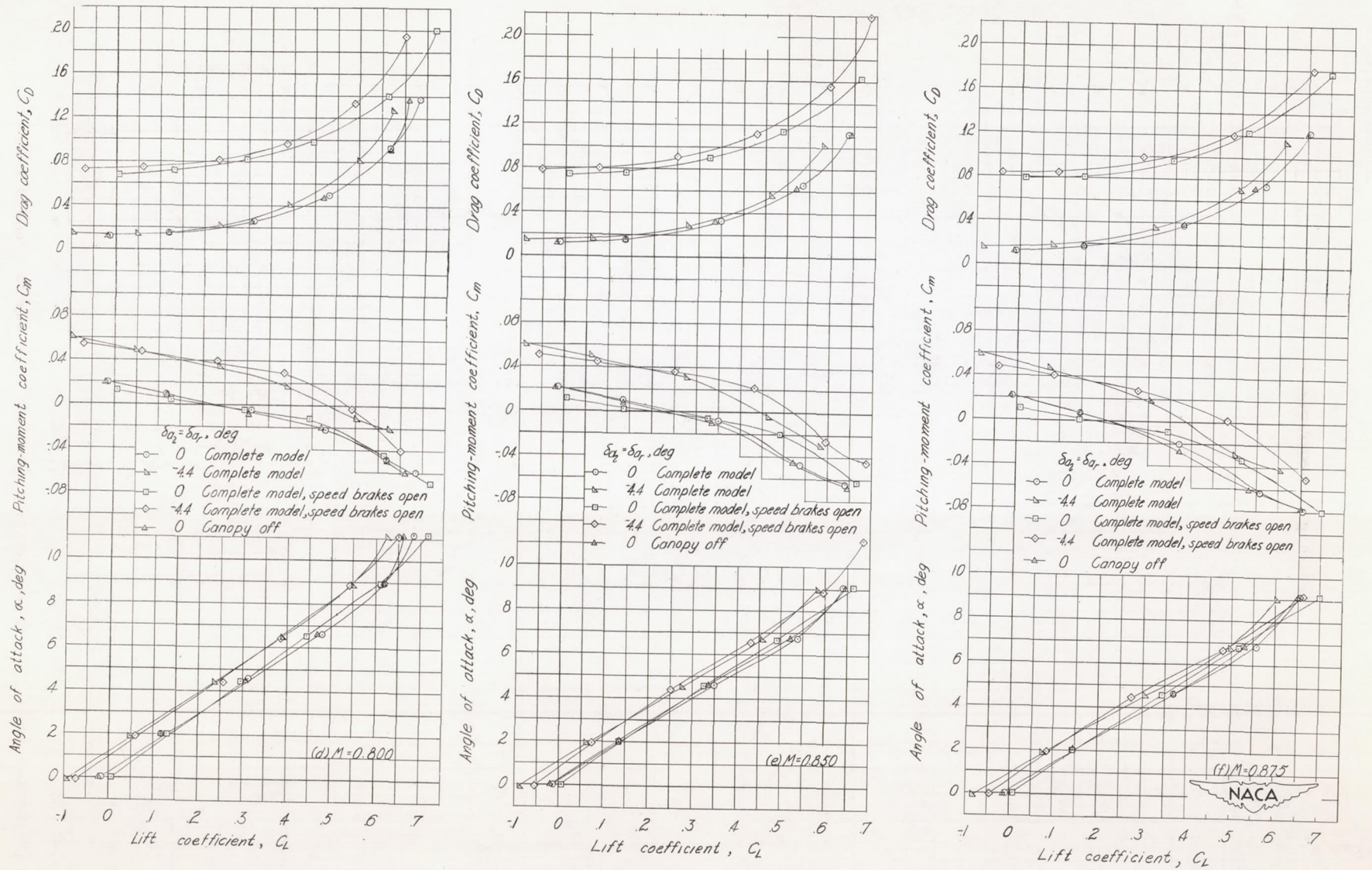

Figure 25.- Continued.

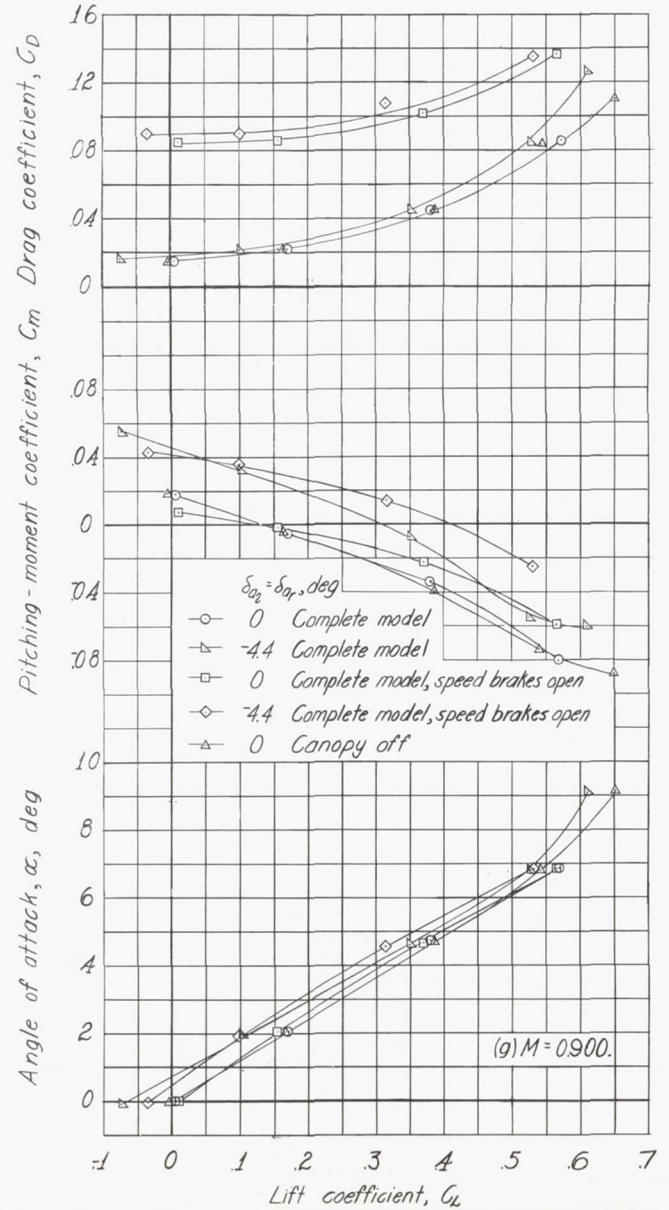

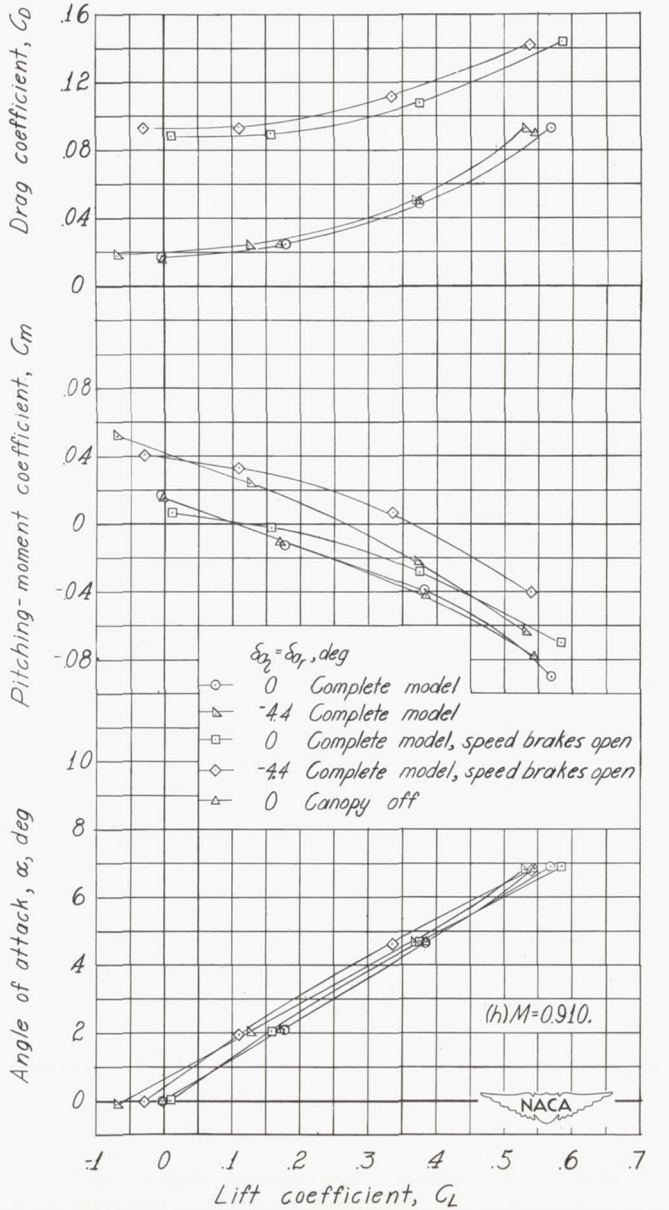

Figure 25. - Concluded.

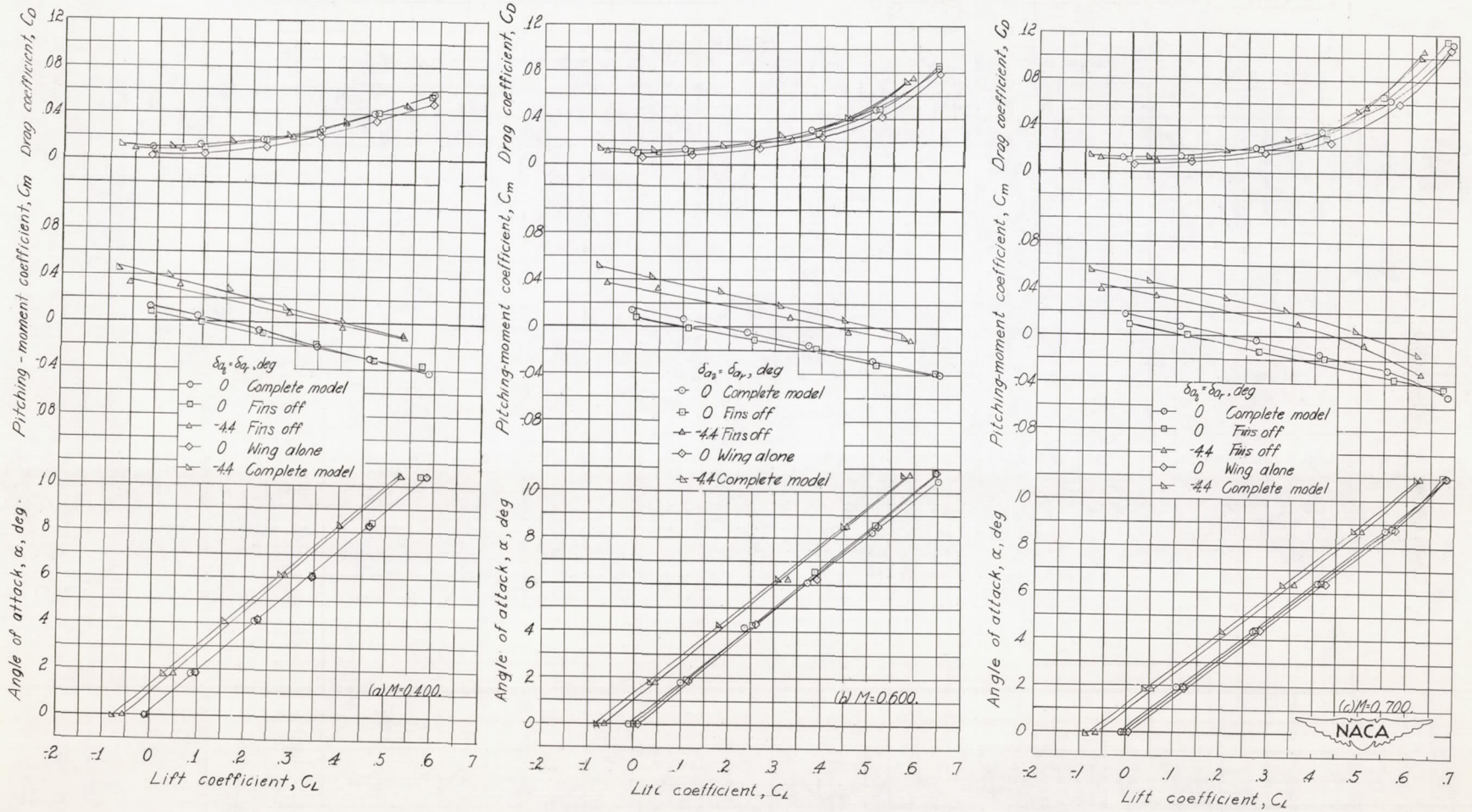

Figure 26.- Fins off and wing alone characteristics of the test model.

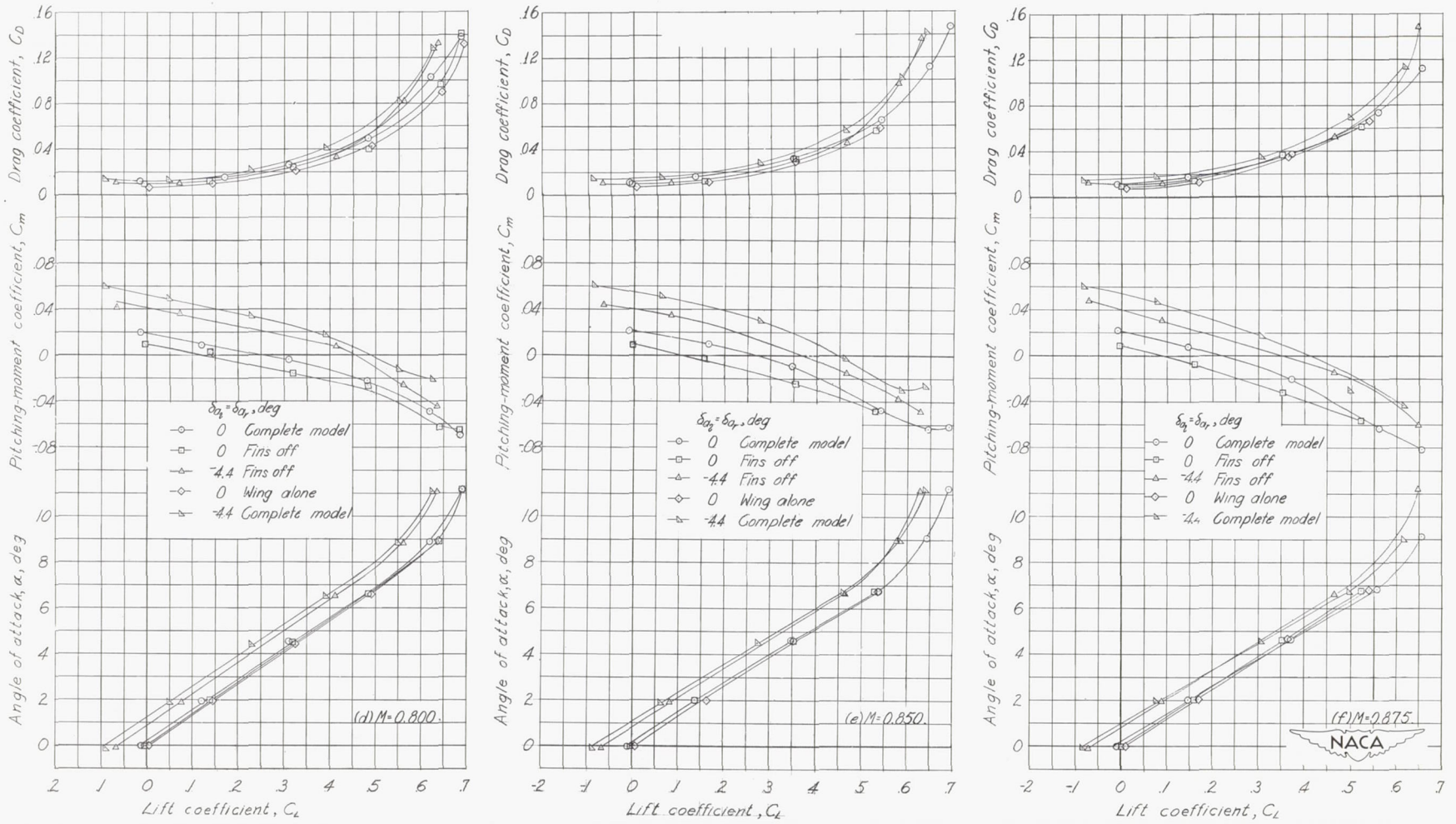

Figure 26.- Continued.

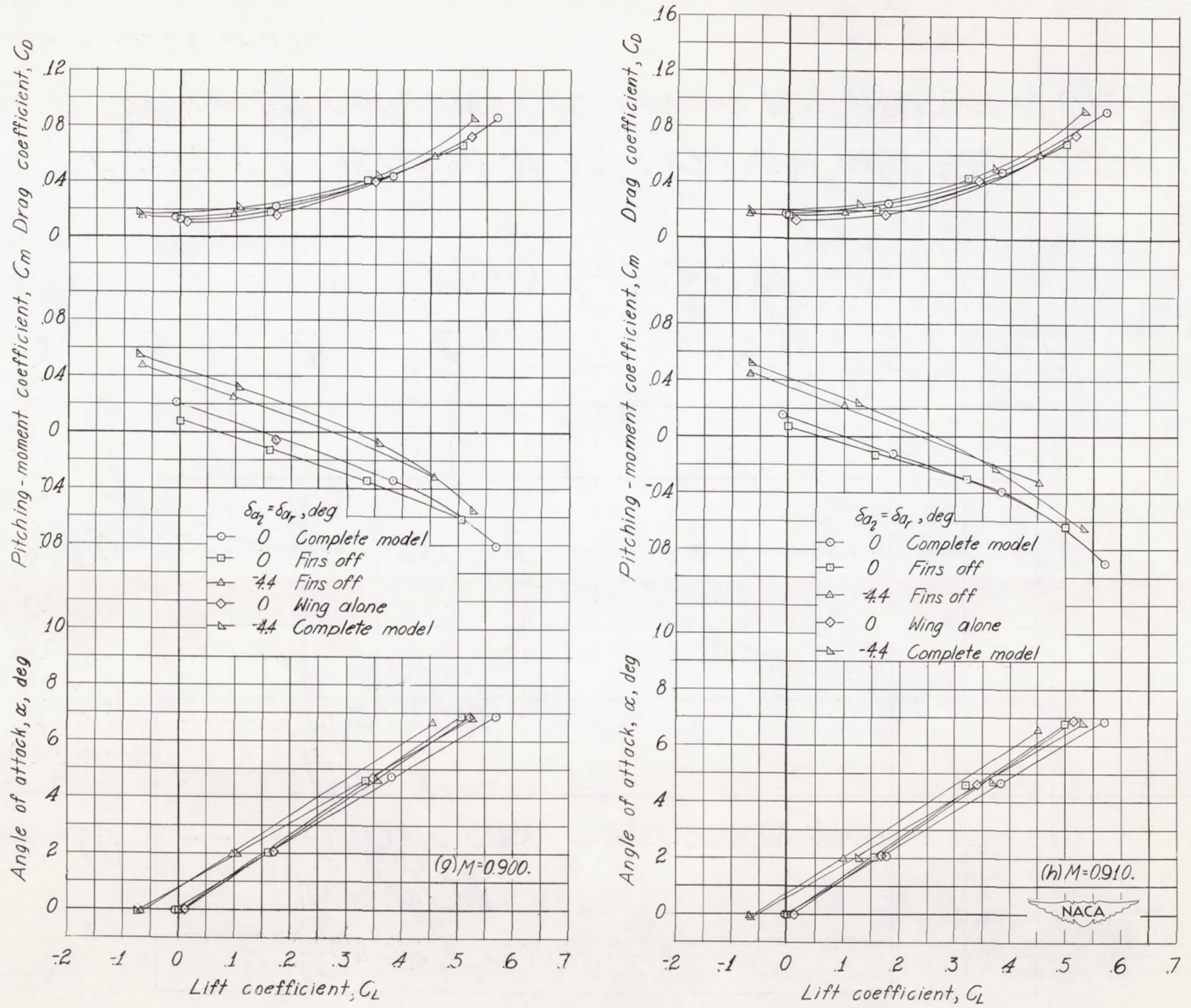

Figure 26.- Concluded.

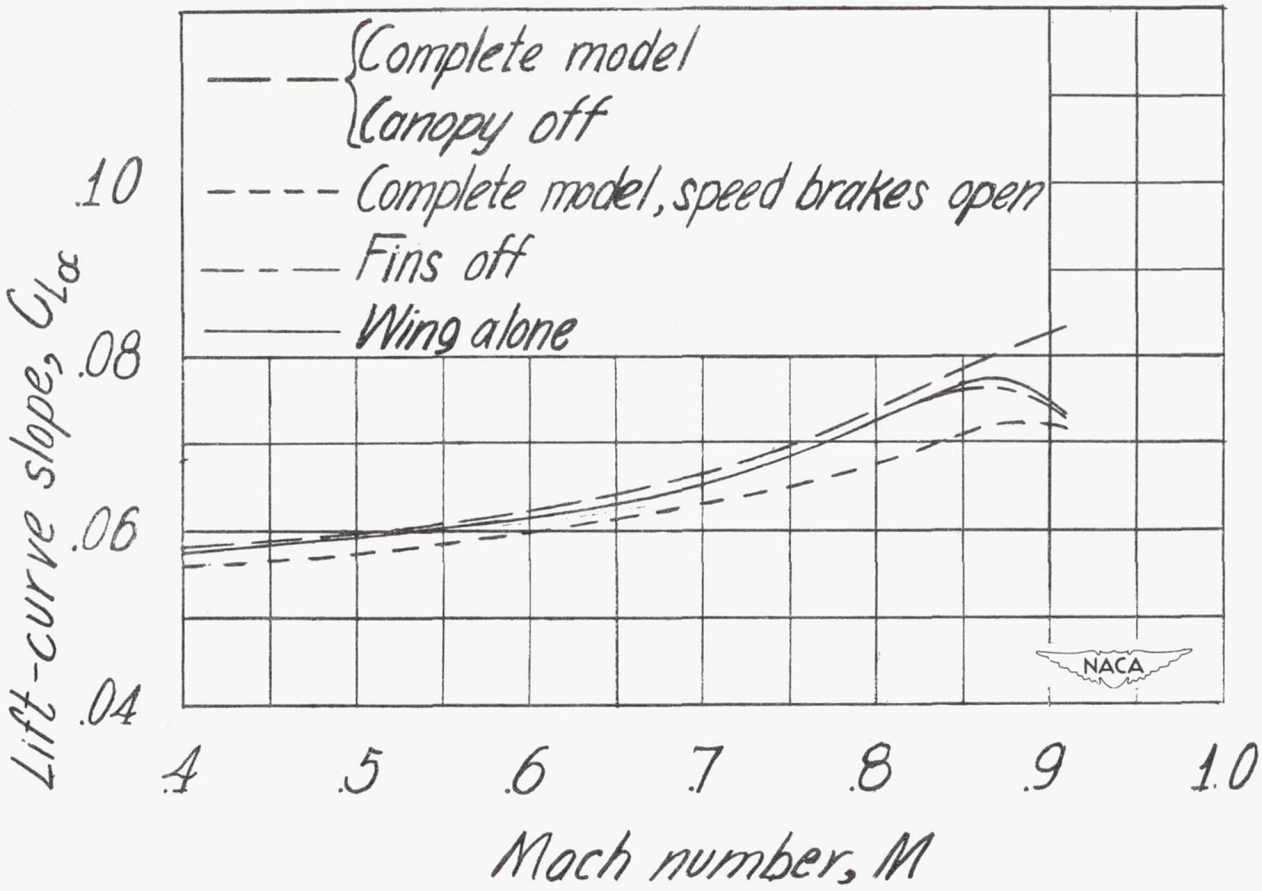

Figure 27.- Variation of lift-curve slope with Mach number for low lift coefficients for various configurations of the test model.

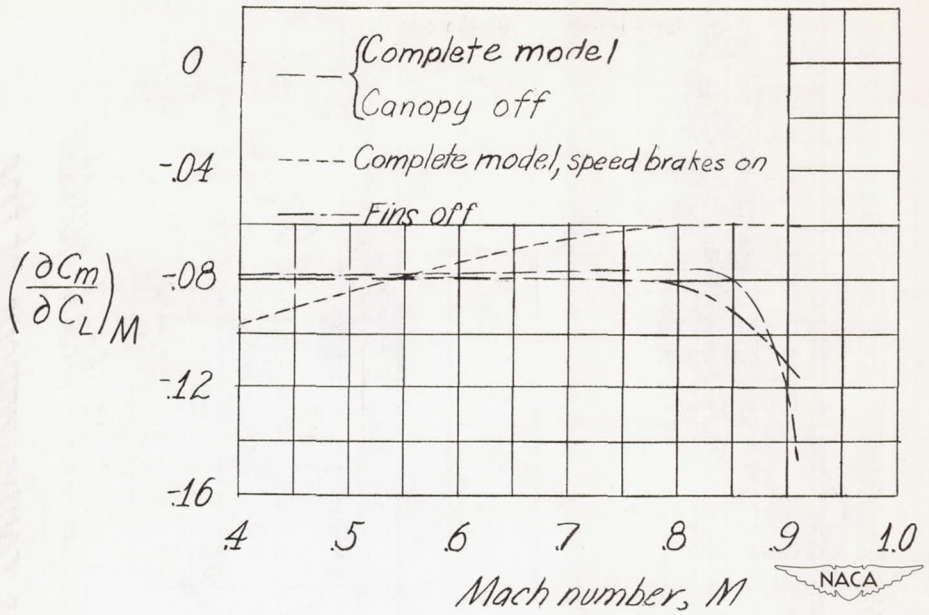

Figure 28.- Variation of $\left(\frac{\partial C_m}{\partial C_L}\right)_M$ with Mach number for the low lift-coefficient range for various configurations of the test model.

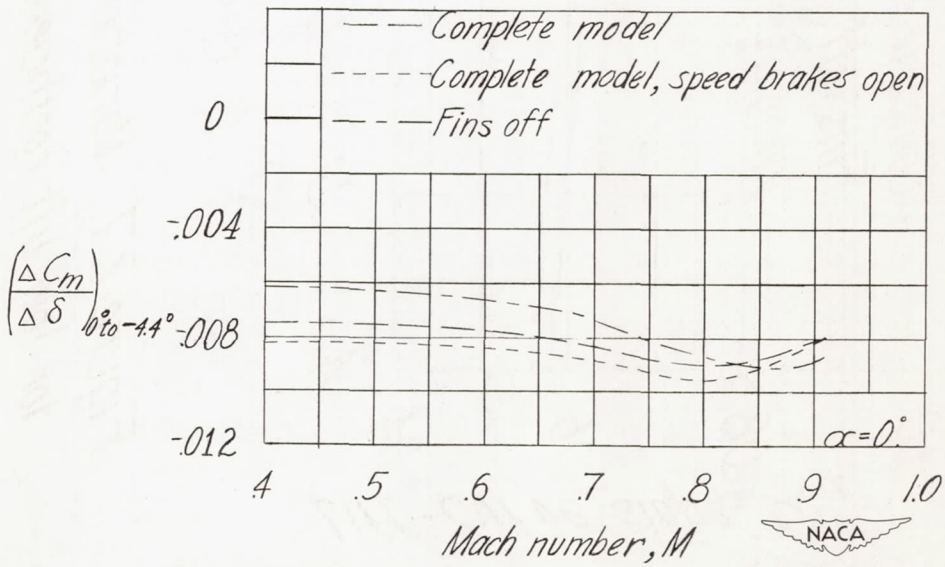

Figure 29.- Variation of the control effectiveness parameter $\left(\frac{\Delta C_m}{\Delta \delta}\right)$ with Mach number for several configurations of the test model.

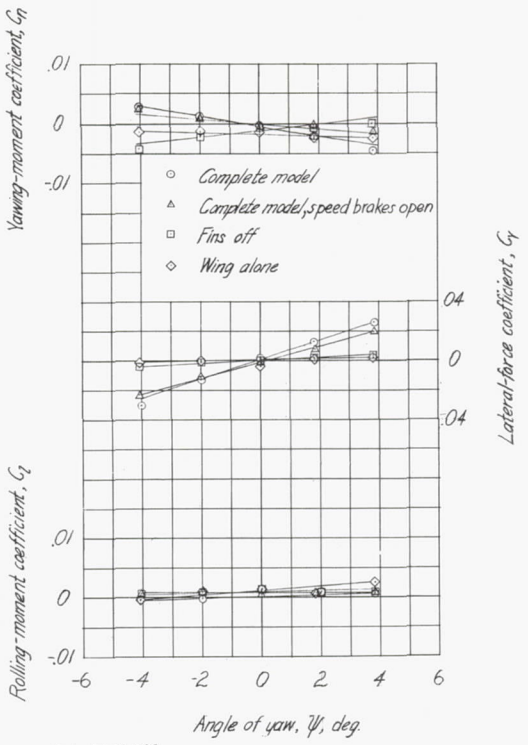

(a) M=0.400.

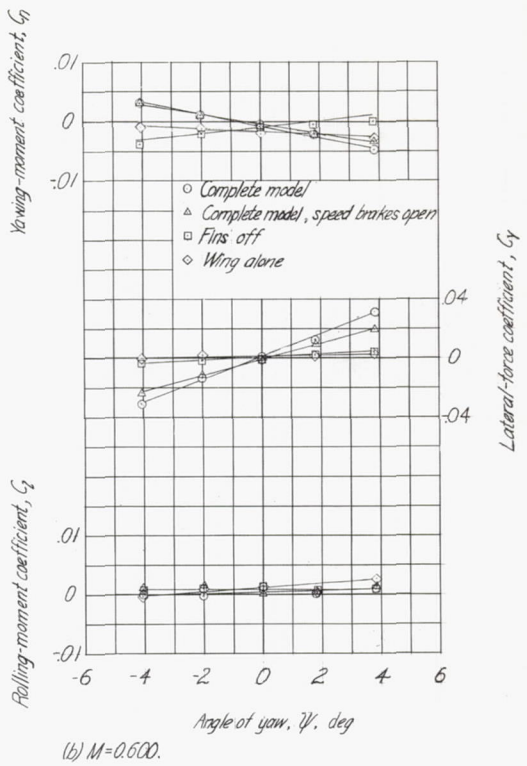

(b) M=0.600.

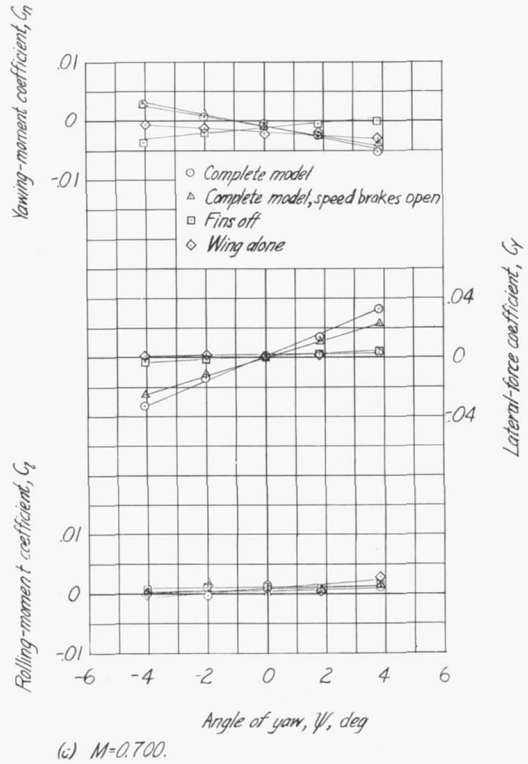

(c) M=0.700.

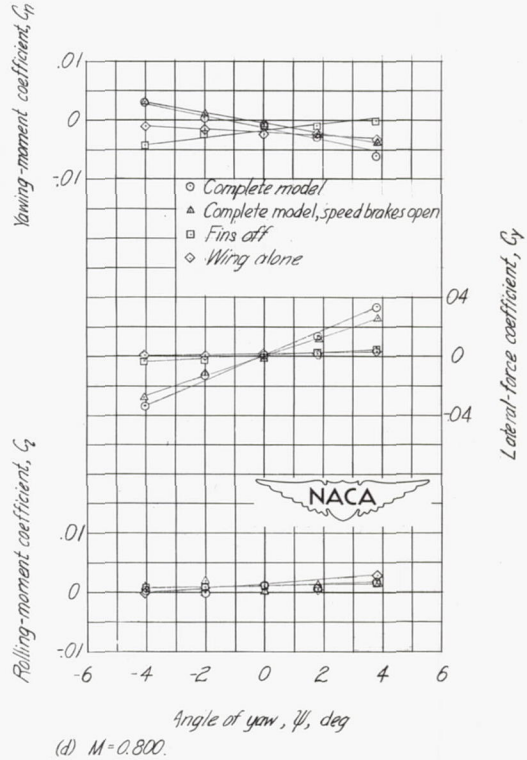

(d) M=0.800.

Figure 30.- Aerodynamic characteristics in yaw for several configurations of the test model; α_{static}=0.

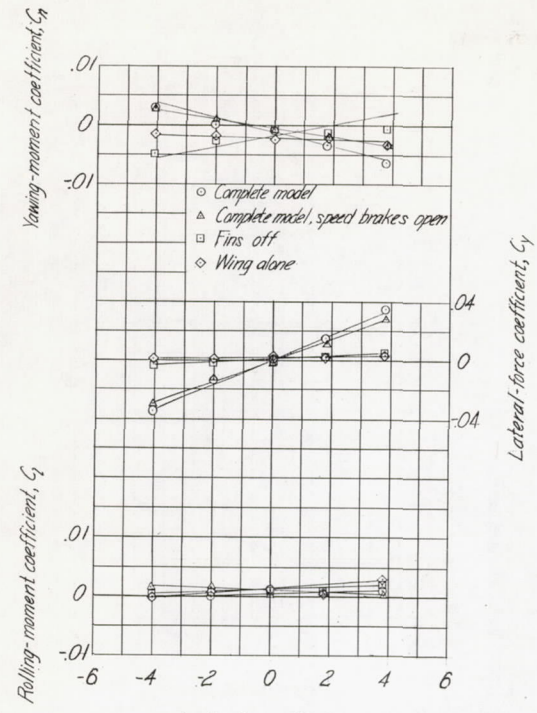

(e) M=0.850.

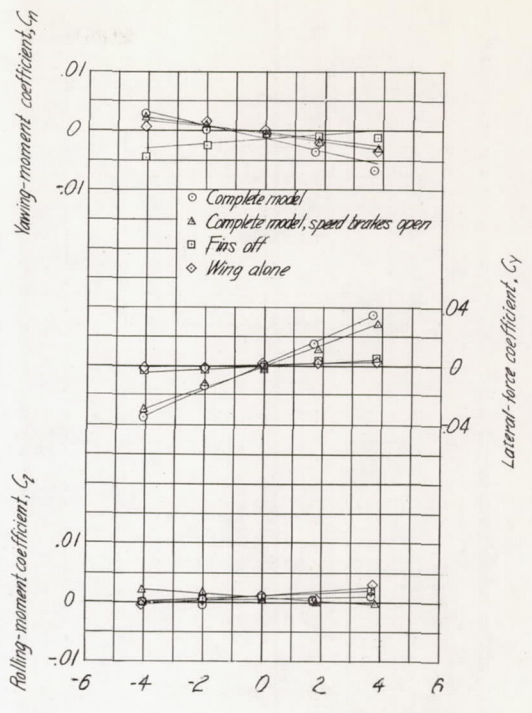

(f) M=0.875.

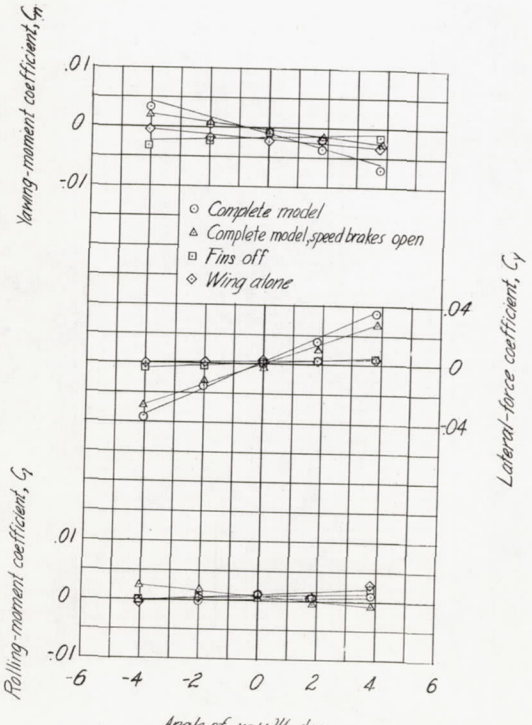

(g) M=0.900.

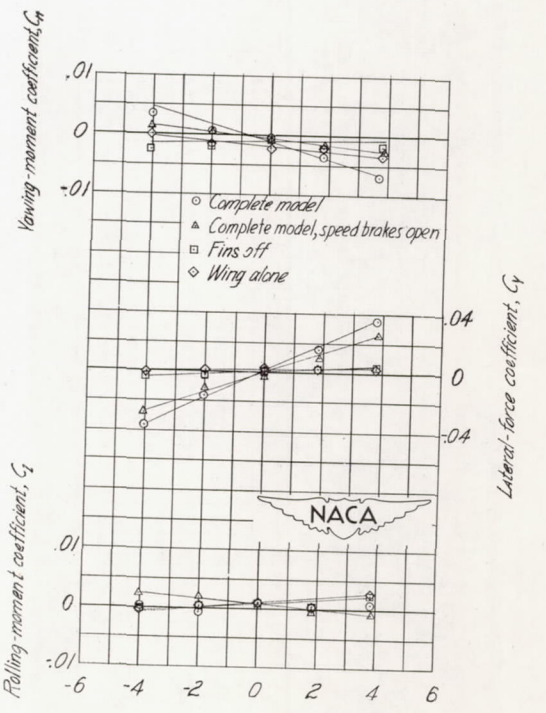

(h) M=0.910.

Figure 30 -Concluded.

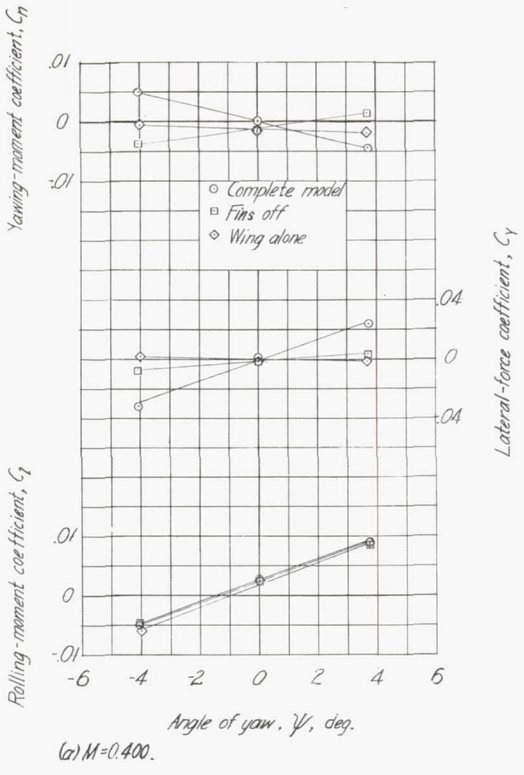

(a) $M = 0.400$.

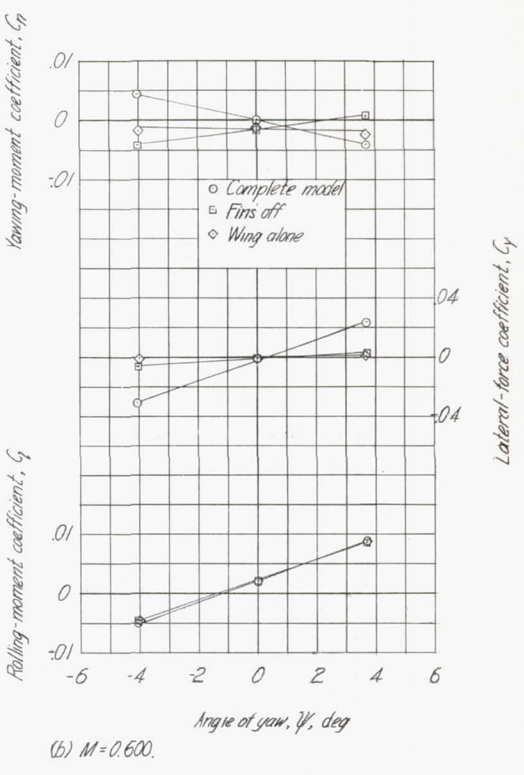

(b) $M = 0.600$.

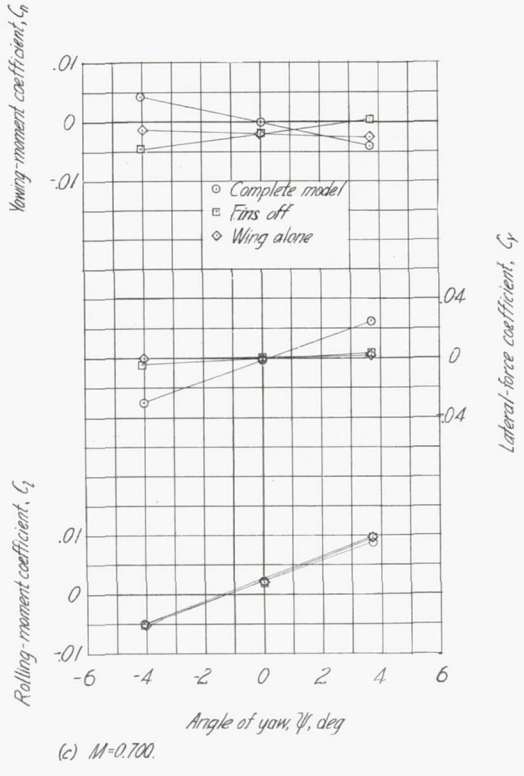

(c) $M = 0.700$.

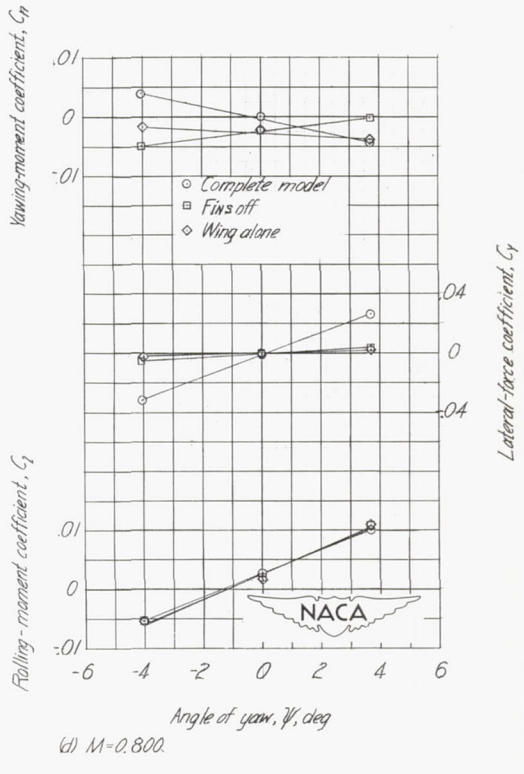

(d) $M = 0.800$.

Figure 31.- Aerodynamic characteristics in yaw for several configurations of the test model; $\alpha_{static} = 6°$

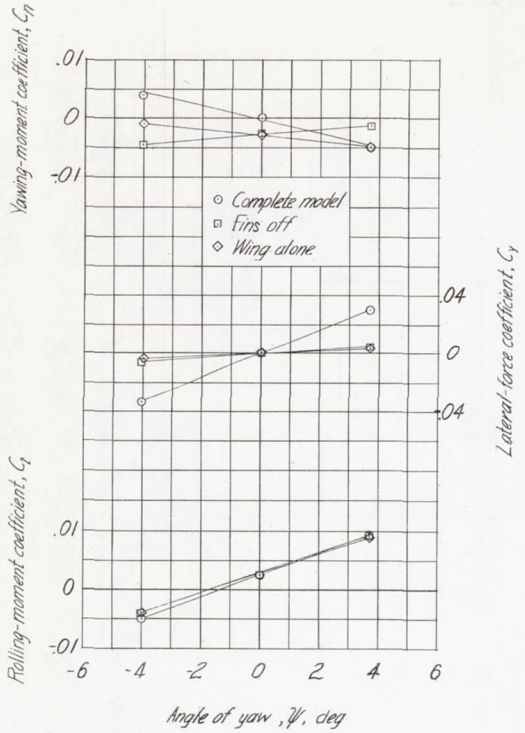

(e) M=0.850.

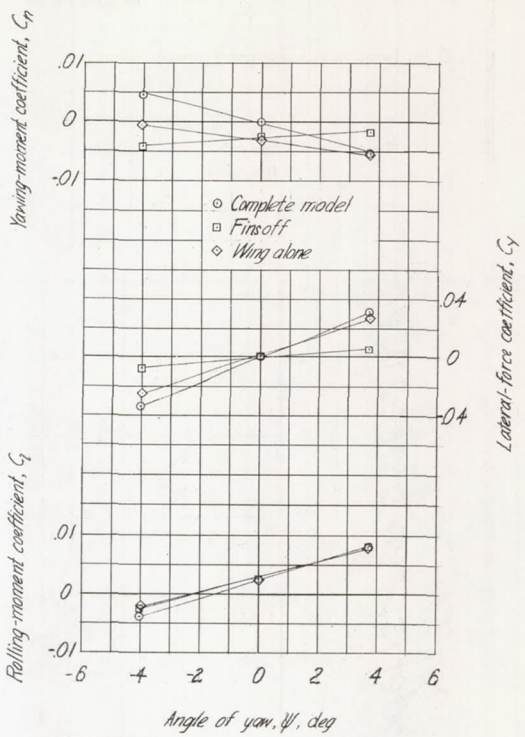

(f) M=0.875.

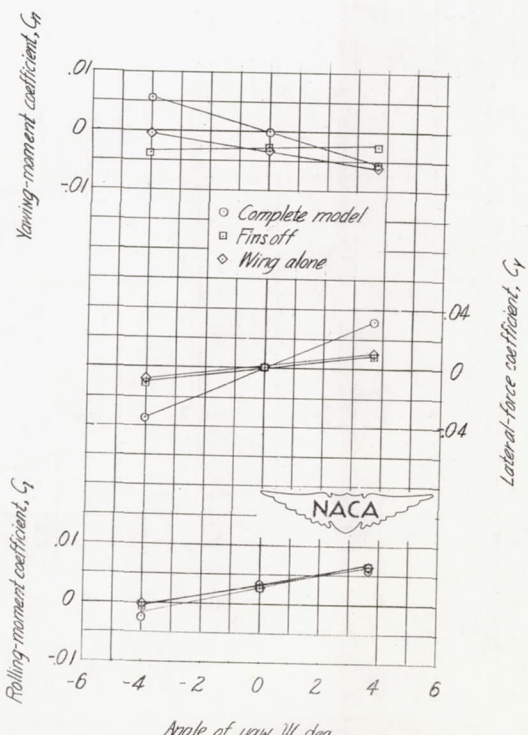

(g) M=0.900

Figure 31 -Concluded

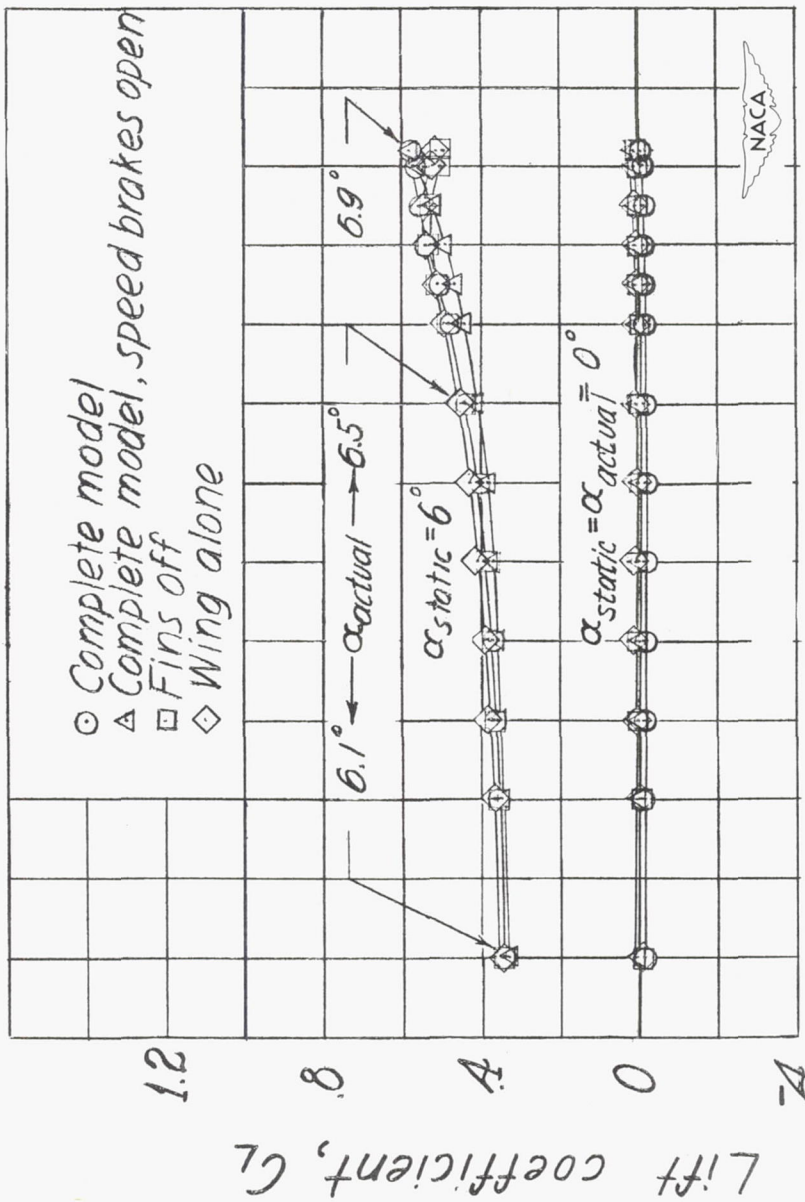

Figure 32-Variation of lift coefficient with Mach number at constant values of static angle of attack for several different model configurations of the test model.

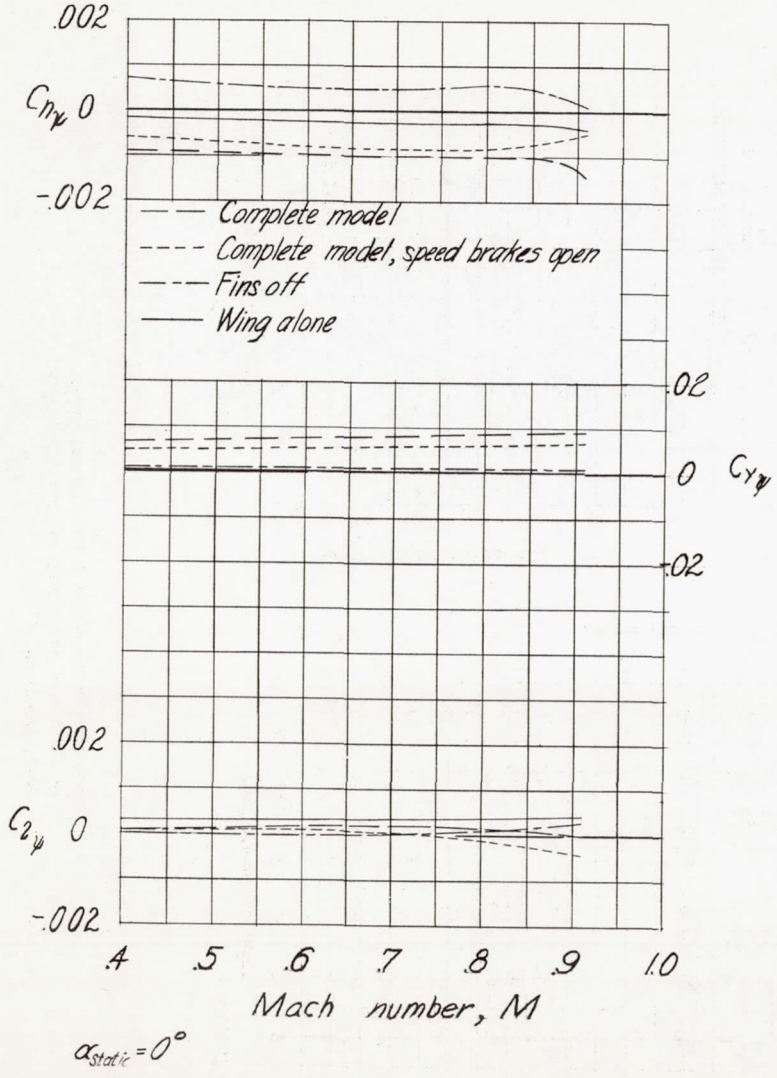

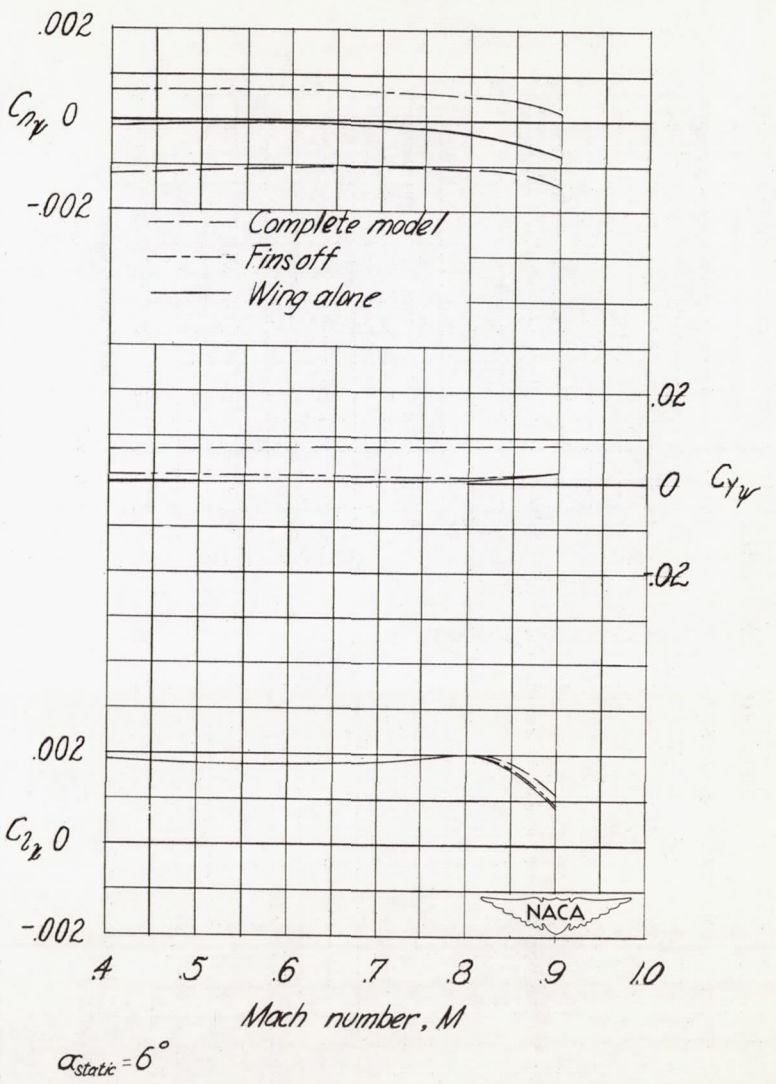

Figure 33.- Variation with Mach number of the lateral stability characteristics for several configurations of the test model.

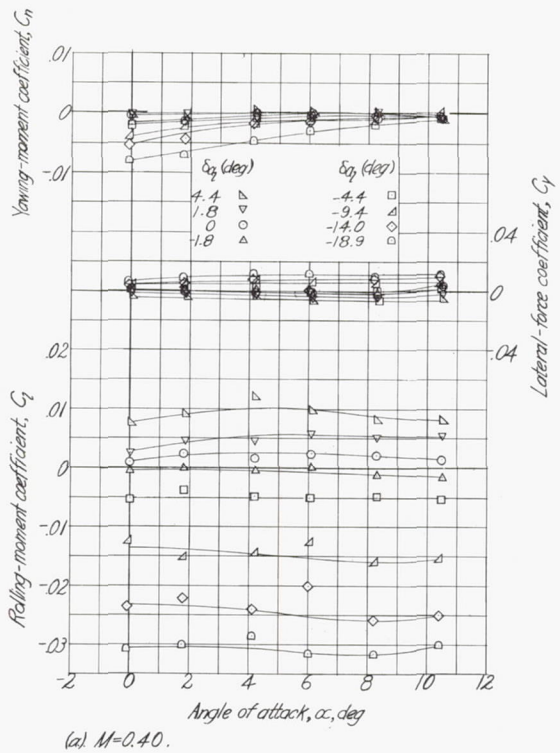

(a) $M = 0.40$.

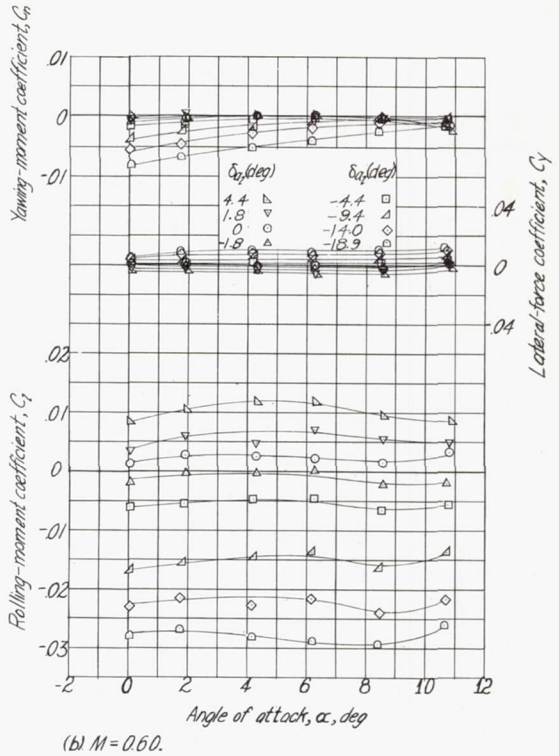

(b) $M = 0.60$.

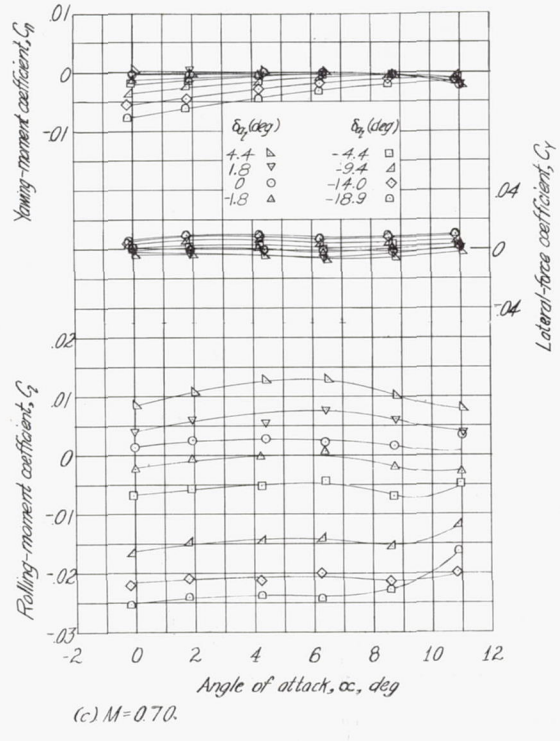

(c) $M = 0.70$.

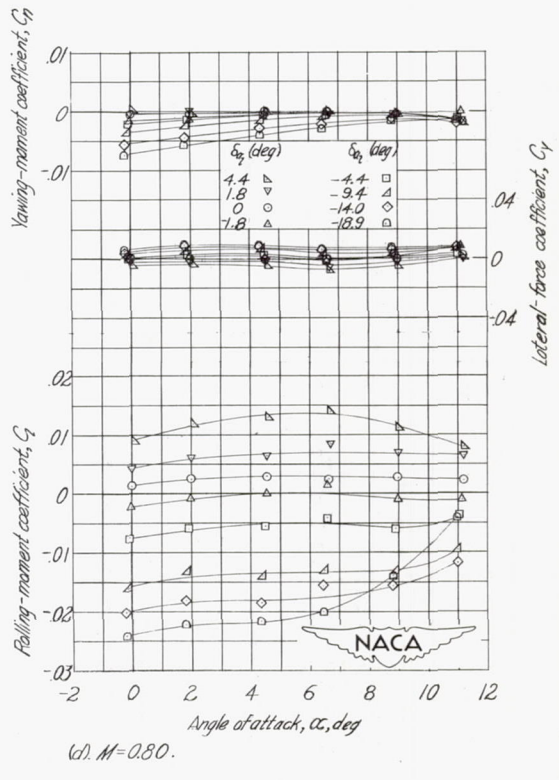

(d) $M = 0.80$.

Figure 34.- Effect of aileron deflection through an angle-of-attack range on the lateral characteristics of the test model. $\delta_{a_r} = 0°$

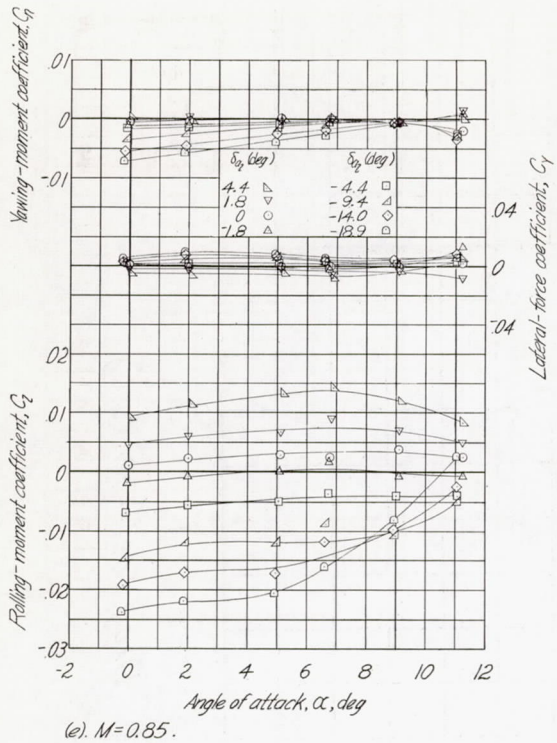

(e). $M = 0.85$.

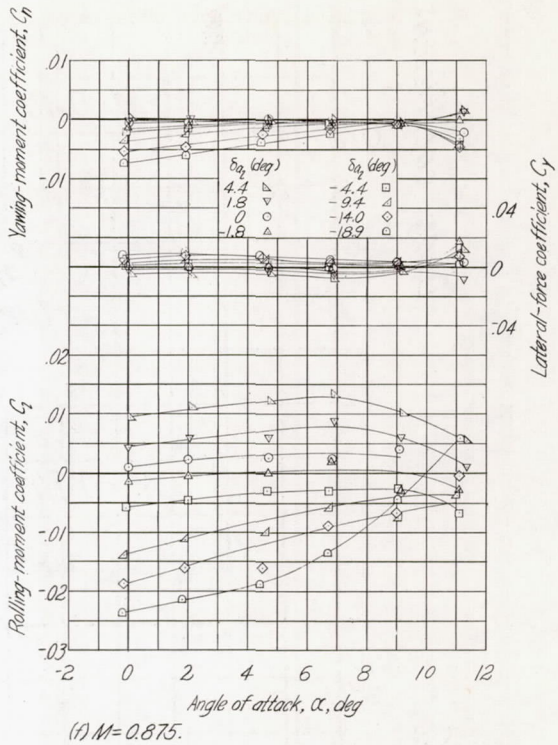

(f) $M = 0.875$.

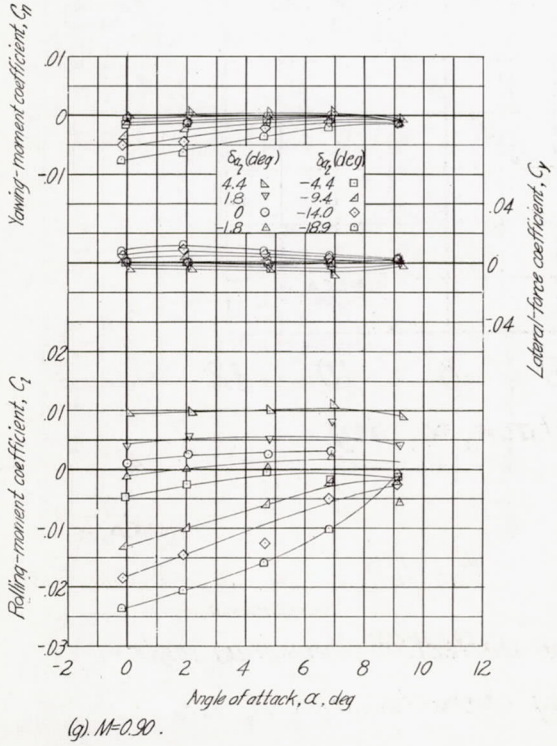

(g). $M = 0.90$.

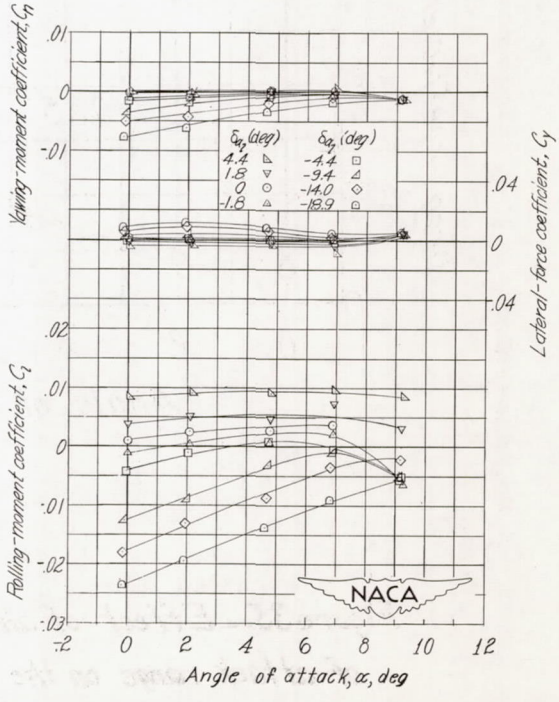

(h). $M = 0.91$.

Figure 34-Concluded.

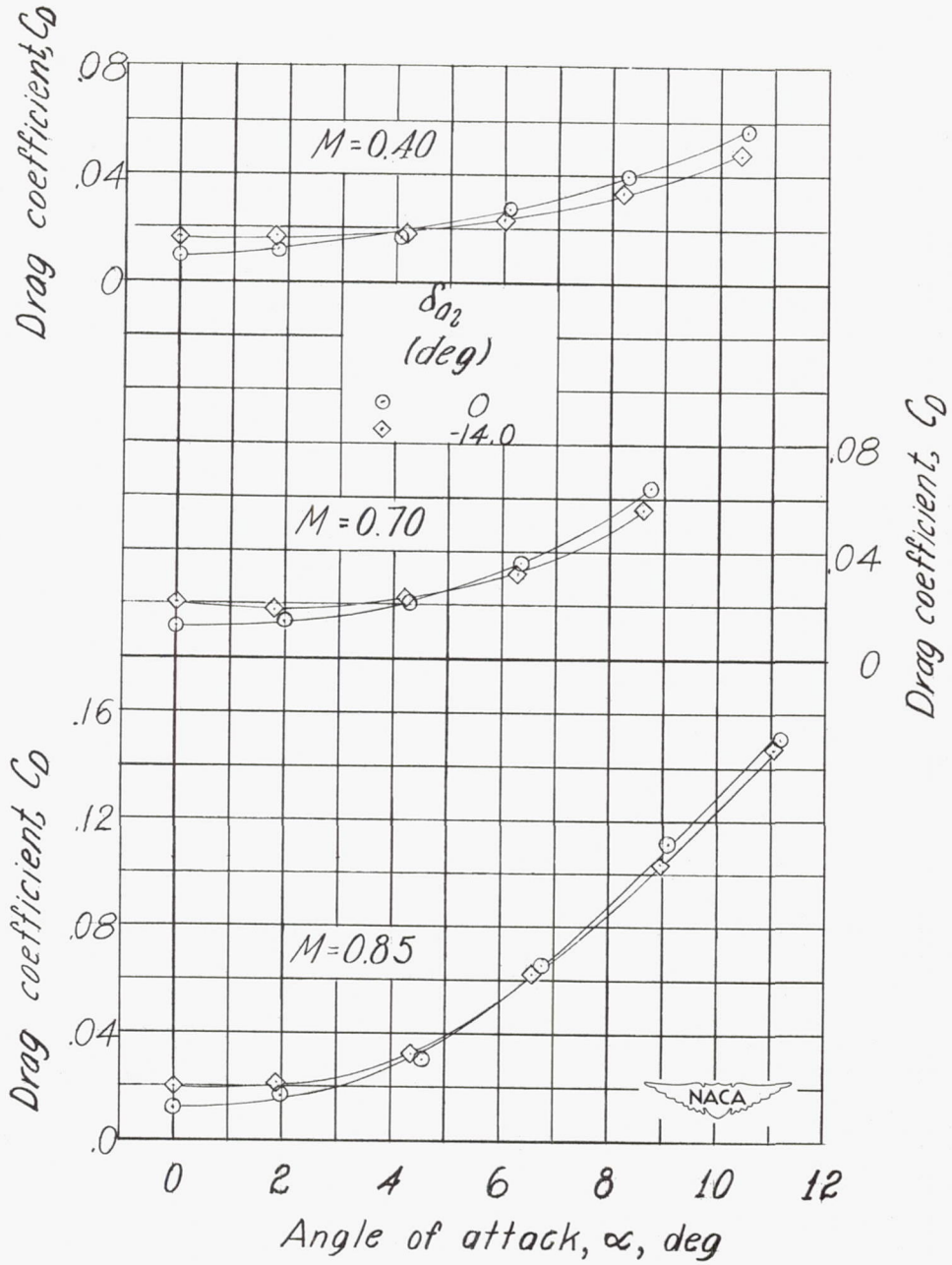

Figure 35.—Effect of aileron deflection through an angle-of-attack range on the drag characteristics of the test model. $\delta_{a_r} = 0°$.

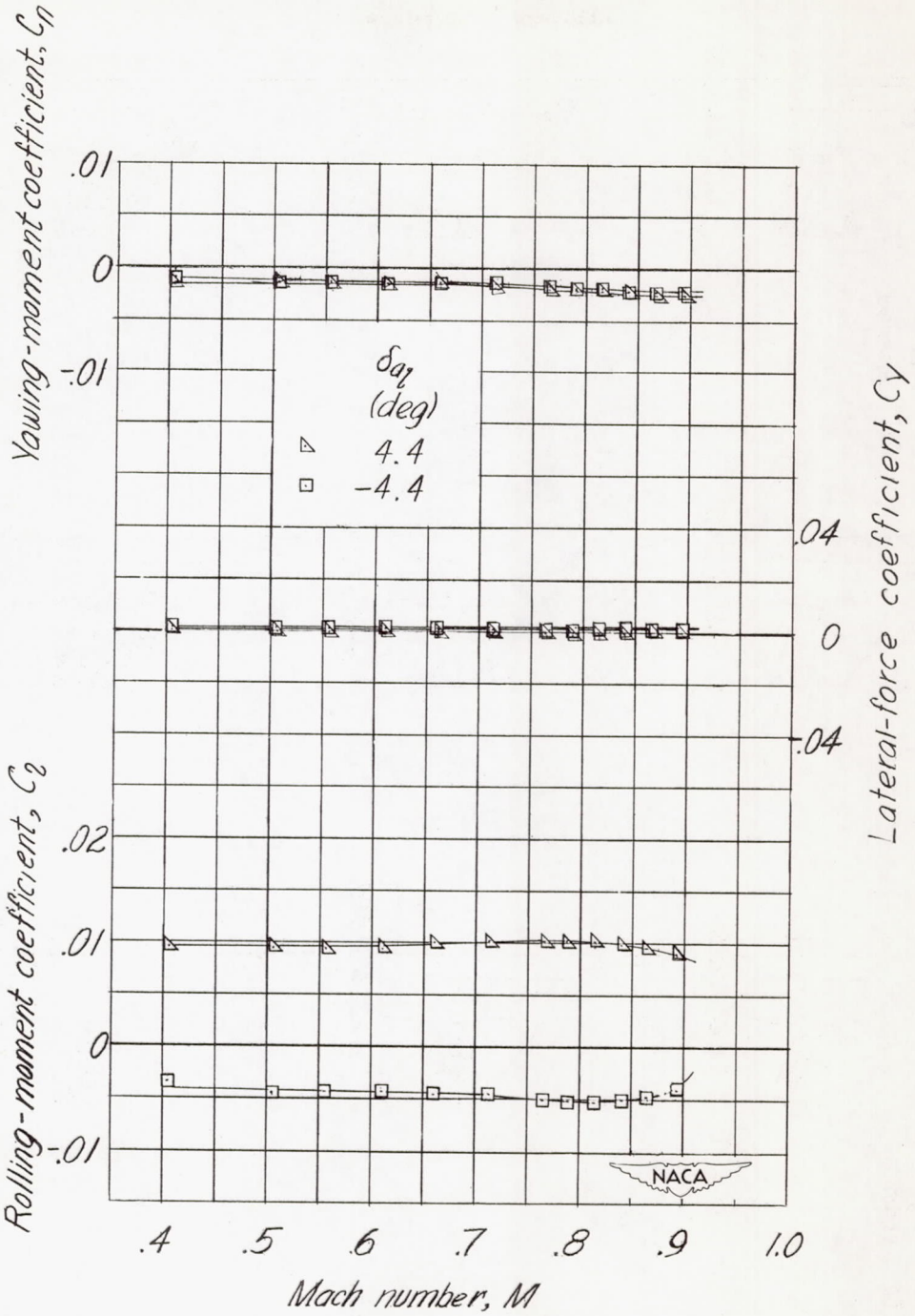

Figure 36.- Effect of aileron deflection through a Mach number range on the lateral characteristics of the test model. $\delta_{a_r} = 0°$; vertical fins off; $\alpha = 1.8°$.

Figure 37.- Tuft studies over the wing at various angles of attack and Mach numbers of the test model. $\Psi = 0°$.

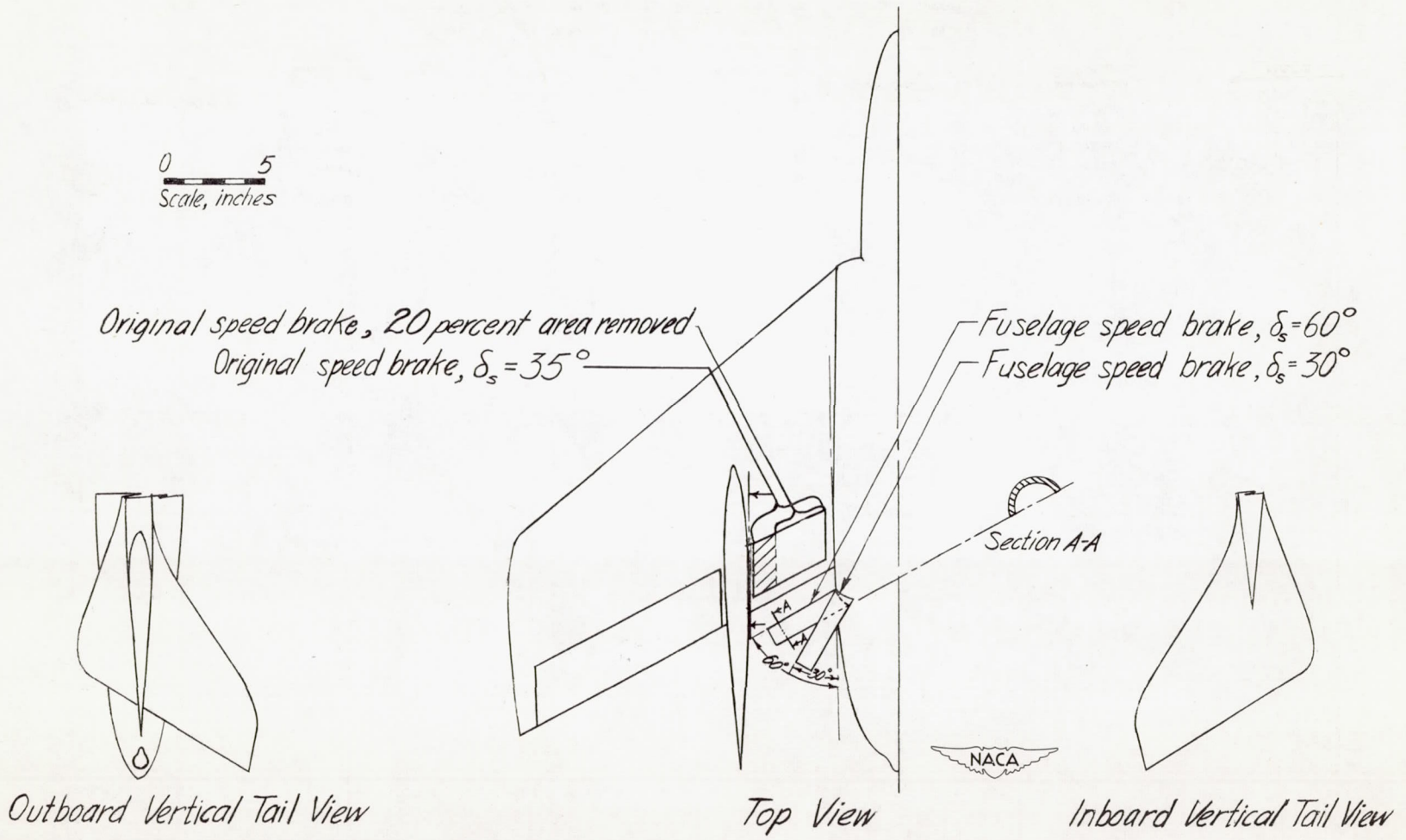

Figure 38.- General arrangement of views for tuft study presentation and the various speed-brake arrangements tested on the test model.

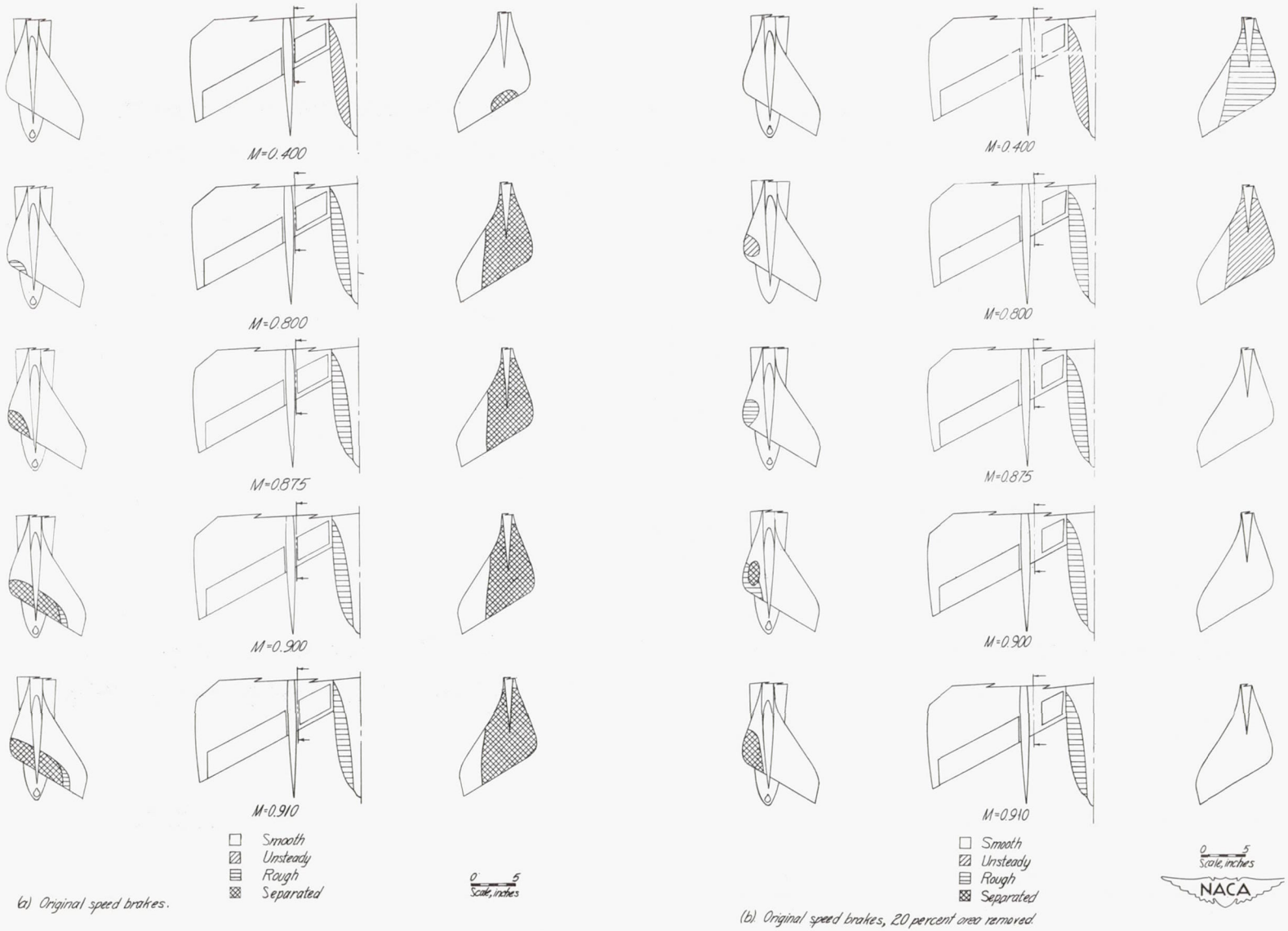

Figure 39.- Tuft studies over the fuselage, outboard vertical fin and inboard vertical fin surfaces at various Mach numbers for the various speed-brake configurations tested; $\alpha = 2°$, $\psi = 0°$.

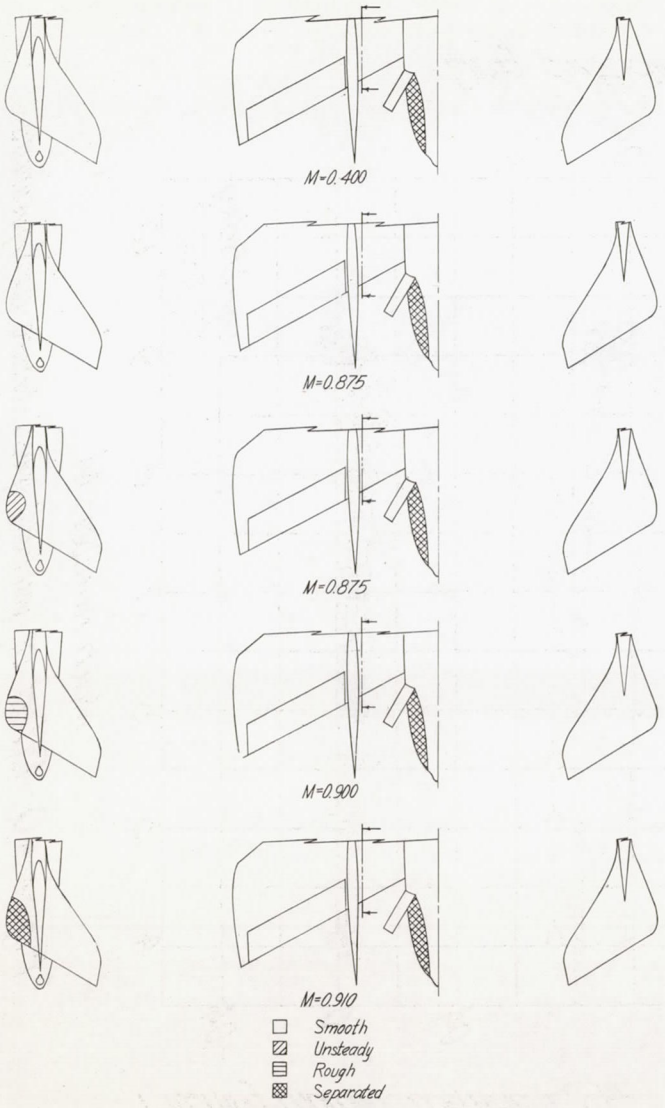

(c) Fuselage speed brakes deflected 30°.

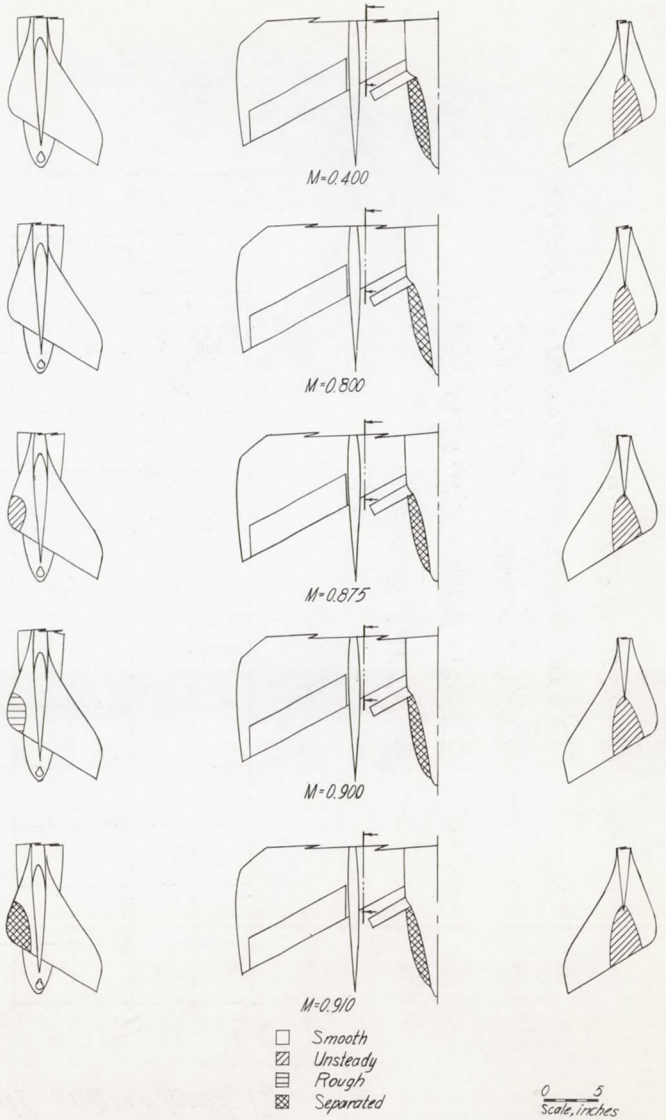

(d) Fuselage speed brakes deflected 60°.

Figure 39.- Concluded.

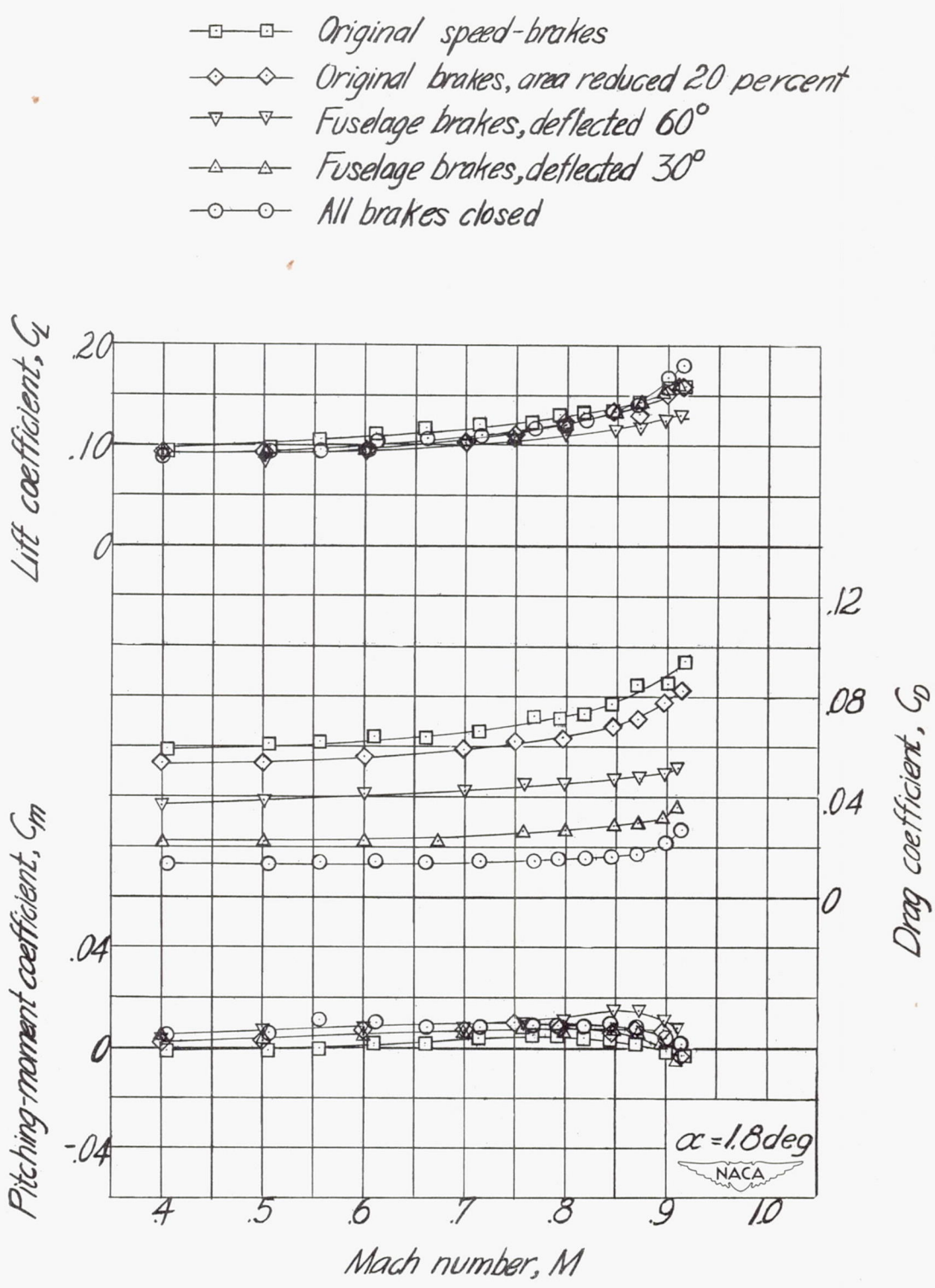

Figure 40.- Effect of various speed-brake configurations on the aerodynamic characteristics in pitch.

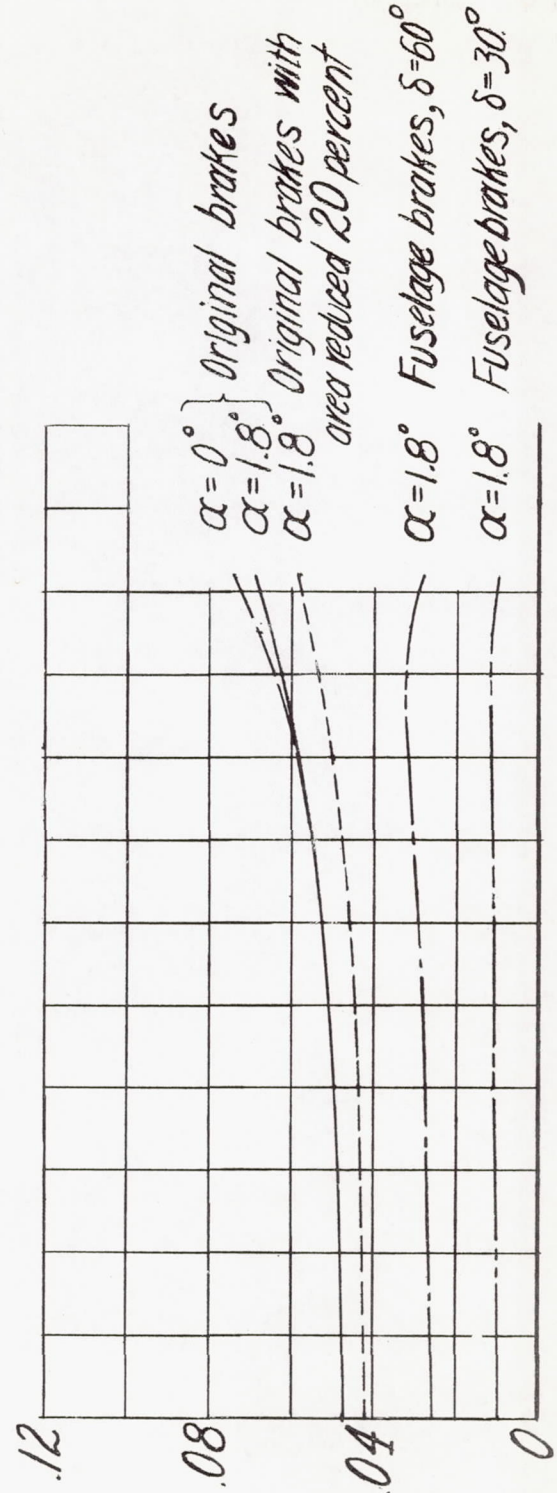

Figure 41.- Variation with Mach number of the drag increments produced by the various speed-brake configurations tested.